

Parametric Modelling of APT Cutters and Accurate Calculation of their Area Moments of Inertia

Guogui Huang

A Thesis

in

the Department

of

Mechanical & Industrial Engineering

Presented in Partial Fulfillment of the Requirements

for the Degree of Master of Applied Science (Mechanical Engineering) at

Concordia University

Montreal, Quebec, Canada

September 2007

© GUOGUI HUANG, 2007



Library and
Archives Canada

Bibliothèque et
Archives Canada

Published Heritage
Branch

Direction du
Patrimoine de l'édition

395 Wellington Street
Ottawa ON K1A 0N4
Canada

395, rue Wellington
Ottawa ON K1A 0N4
Canada

Your file Votre référence

ISBN: 978-0-494-40911-4

Our file Notre référence

ISBN: 978-0-494-40911-4

NOTICE:

The author has granted a non-exclusive license allowing Library and Archives Canada to reproduce, publish, archive, preserve, conserve, communicate to the public by telecommunication or on the Internet, loan, distribute and sell theses worldwide, for commercial or non-commercial purposes, in microform, paper, electronic and/or any other formats.

The author retains copyright ownership and moral rights in this thesis. Neither the thesis nor substantial extracts from it may be printed or otherwise reproduced without the author's permission.

AVIS:

L'auteur a accordé une licence non exclusive permettant à la Bibliothèque et Archives Canada de reproduire, publier, archiver, sauvegarder, conserver, transmettre au public par télécommunication ou par l'Internet, prêter, distribuer et vendre des thèses partout dans le monde, à des fins commerciales ou autres, sur support microforme, papier, électronique et/ou autres formats.

L'auteur conserve la propriété du droit d'auteur et des droits moraux qui protège cette thèse. Ni la thèse ni des extraits substantiels de celle-ci ne doivent être imprimés ou autrement reproduits sans son autorisation.

In compliance with the Canadian Privacy Act some supporting forms may have been removed from this thesis.

Conformément à la loi canadienne sur la protection de la vie privée, quelques formulaires secondaires ont été enlevés de cette thèse.

While these forms may be included in the document page count, their removal does not represent any loss of content from the thesis.

Bien que ces formulaires aient inclus dans la pagination, il n'y aura aucun contenu manquant.



Canada

Abstract

Parametric Modeling of APT Cutters and Accurate Calculation of their Area Moments of Inertia

Guogui Huang

Due to cutting forces and the flexibility of the tool and its holder, the tool (or end-mill) deflects when it is engaging with the workpiece; unfortunately, large deflections can cost part accuracy, even break the tool. To produce high-precision parts, it is important to predict the deflections with high fidelity and then greatly reduce them through compensation in CNC tool paths. For this purpose, many research works have been successfully conducted on cutting forces prediction; however, another critical factor, the area moment of inertia of the tool, is always approximated, significantly reducing the accuracy of estimated deflections. The main reason for this is that the 3-D geometric model of end-mills is difficult to construct. To find the moment of inertia, in this work, first, a parametric model of APT cutters has been established and implemented in the CATIA CAD/CAM system by using its API. Then, a system of calculating the area moment of inertia for end-mills is built. Finally, a detailed discussion on the moment of inertia of end-mills is provided, along with comparison of this work with the existing methods. The major contributions of this work include the parametric end-mill modeling, which can automatically render the 3-D geometric model of an end-mill in seconds, and accurate calculation of the moments of inertia of end-mills. This work can be used, together with an existing cutting force calculation method, to accurately predict cutter deflections during milling in order to compensate them in CNC tool paths. It can also

provide more precise 3-D solid models of end-mills for machining simulation by using finite element analysis.

Acknowledgements

I would like to say thanks to my supervisor, Dr. Zezhong C. Chen, for his guidance and support for this research topic. I really appreciate his enthusiasm, encouragement, expertise, and research philosophy. To Qiang Fu, Hong Da Zhang, Saeed Al-Taher, Maqsood, Tian Bo Zhao, Gang Liu, and Hong Zheng, I give my thanks for their encouragement, their valuable insight, and their comments.

Tables of Contents

List of Figures	viii
List of Tables	x
 Chapter 1 Introduction	 1
1.1 Introduction and Review of CAD	1
1.1.1 Definition of Computer Aided Design (CAD)	1
1.1.2 CAD Background	2
1.1.3 Fields of CAD Application and Capabilities	3
1.1.4 Advantages of CAD	6
1.2 Parametric Design	7
1.2.1 Definition of Parametric Design	7
1.2.2 Parametric Design	8
1.3 Area Moment of Inertia	9
1.4 Literature Review	10
1.5 Research Objectives	12
1.6 Thesis Outline	13
 Chapter 2 Parametric Representation of the Cutting Edges of APT Cutters	 14
2.1 Nomenclature	14
2.2 Parametric Representation of the Envelopes of APT Cutters	15
2.2.1 Parametric Equation of the Conic Surface	18
2.2.2 Parametric Equation of the Fillet	19
2.2.3 Parametric Equation of the Taper	19
2.3 Parametric Representation of the Helical Cutting Edge	20
2.3.1 Helical Segment on the Conic Surface	20
2.3.2 Helical Segment on the Fillet	24
2.3.3 Helical Segment on the Taper	28
2.4 Non Tangential Conditions	32

Chapter 3	Representation of Cutter Flutes	33
3.1	The Coordinates of the Intersection Points of the Profile of Cutting Flute.....	34
3.2	Polar Equations of the Flute Segments.....	39
3.3	Program and the 3D Models of Cutting Tools	44
Chapter 4	Accurate Calculation of Area Moments of Inertia of APT Cutters	48
4.1	Representation of Polar Angle	49
4.2	Difference of Polar Angle between Segments of Sectional Flute	50
Chapter 5	Analysis and Comparison	60
5.1	Introduction	60
5.2	Influence of the Cutting Flutes	60
5.3	Influence of the Other Parameters	63
5.4	Along the Tool Axis, Different Position, Different Area Moment of Inertia	65
Chapter 6	Results and Application	73
6.1	Introduction	73
6.2	Applications.....	73
Chapter 7	Conclusions and Future Research	76
7.1	Conclusions	76
7.2	Future Research.....	77
Chapter 8	Appendix	78
Chapter 9	Bibliography	84

List of Figures

Figure 2-1 Schematic of the envelope of an APT cutter in the tool coordinate system.	16
Figure 3-1 Sectional View of a Flute.....	34
Figure 3-2 Parameters Interface.....	44
Figure 3-3 Flat End Mill	45
Figure 3-4 Ball Nose End Mill.....	46
Figure 3-5 Bull Nosed End Mill	46
Figure 3-6 Apt Cutting Tool	47
Figure 4-1 Diagram of one of the cutter flute.	49
Figure 5-1 Area Moment of Inertia vs. Flutes.	62
Figure 5-2 Area Moment of Inertia vs. Flutes.	62
Figure 5-3 The Effect of r_0	64
Figure 5-4 Area Moment of Inertia $\sim z$	68
Figure 5-5 Area Moment of Inertia $\sim z$	68
Figure 5-6 Area Moment of Inertia $\sim z$	69
Figure 5-7 Area Moment of Inertia $\sim z$	71
Figure 5-8 Area Moment of Inertia $\sim z$	71
Figure 5-9 Area Moment of Inertia of a 2-tooth Apt Cutting Tool $\sim z$	72
Figure 5-10 Area Moment of Inertia $\sim z$	72

List of Tables

Table 5-1 Area of Moment of Inertia of Different End-Mills	61
Table 5-2 Comparison of the Effect of the Radius of Annular Land r_0 on the Inertia.....	64
Table 5-3 The Effect of r_1 , r_2 and Rake Angle, α , and Relief Angle	65
Table 5-4 Data for Symmetric and Asymmetric Section Flat-End Mills	67
Table 5-5 Data for Symmetric and Asymmetric Section APT Cutting Tool.....	70
Table 6-1 Equivalent Radius for 2-Flute Cutters.....	74
Table 6-2 Equivalent Radius for 3-Flute Cutters.....	75
Table 6-3 Equivalent Radius for 4-Flute Cutters.....	75

Chapter 1 Introduction

1.1 Introduction and Review of CAD

1.1.1 Definition of Computer Aided Design (CAD)

CAD is the abbreviation of Computer Aided Design, which originally meant Computer Aided Drafting, because, in the early days, CAD was really a replacement for traditional drafting boards. Now, CAD usually reflects the functions with which the modern CAD tools can do much more than drafting. It is the technology concerned with the use of computer systems to assist in creation, modification, analysis, and optimization of a design [Flute and Zimmers, 1984]. Thus any computer program, which embodies computer graphics and an application program facilitating engineering functions in a design process, is classified as CAD software. In other words, CAD tools can vary from geometric tools for manipulating shapes at one extreme, to customized application programs, such as those for analysis and optimization, at the other extreme [Zeid, 1991]. Each of the different types of CAD systems require the manipulator to think in a different way about how he/she will use them and he/she must design their virtual components in a different manner. Products under CAD design are convenient to FEM analysis for design

optimization, and convenient to next engineering process, such as die/mould design and machining programming and simulation.

1.1.2 CAD Background

Initial developments of CAD were carried out in the 1960s within the aircraft and automotive industries in the area of 3-D surface modeling, construction and NC programming, most of which are independent of one another and often not publicly published at that time. It was not until much later, some of the mathematical description work on curves was developed by Isaac Jacob Schoenberg, Apalatequi (Douglas Aircraft) and Roy Liming (North American Aircraft). However, probably the most important work is the descriptions on polynomial curves and sculptured surface, which were done by Pierre Bezier (Renault) and Paul de Casteljaou (Citroen).

First commercial application of CAD was in large companies in the automotive and aerospace industries, as well as in electronics, since only large corporations could afford the computers capable of performing the massive calculations on graphics. One of the most influential growths in the development of CAD was the founding of MCS (Manufacturing and Consulting Services Inc.) in 1971 by Dr. P. J. Hanratty, who wrote the system ADAM (Automated Drafting and Machining). As computers became more affordable, the application of CAD and its application areas have gradually expanded. The development of PC is the impetus of the development of CAD software for almost universal application in all areas, and because of the development of PC, CAD implementations have grown dramatically since then.

In the CAD development history, the key products were the solid modeling packages- Romulus (ShapeData) and Uni-Solid (Unigraphics) based on PADL-2 and the release of the surface modeler CATIA (Dassault System). The next milestone was the release of Pro/Engineer in 1988, which mostly used feature-based modeling methods and parametric linking of the constraints and relations of features. Another importance to the development of CAD was the development of the Boundary-representation (B-rep) solid modeling kernels (engines for manipulating geometrically and topologically consistent 3D objects) by Parasolid (ShapeData) and ACIS (Spatial Technology Inc.) at the end of the 1980s and beginning of 1990s, both inspired by the work of Ian Braid. This led to the release of mid-range packages CAD such as SolidWorks in 1995, SolidEdge (Intergraph) in 1996, and IronCAD in 1998. Today, CAD is one of the main tools used in designing products.

1.1.3 Fields of CAD Application and Capabilities

Thanks to development of PCs which can be afforded by most of the industries, not just for large industries anymore, and development of description works on curves and surfaces, CAD software products now are booming.

The different application areas of CAD include:

1. The AEC industry- architecture, engineering and construction

- Architecture
- Building engineering

- Civil engineering and infrastructure
- Construction
- Road and highways
- Railroad and tunnels
- Water supply and hydraulic engineering
- Storm drain, wastewater and sewer systems
- Mapping and surveying
- Plant design
- Factory layout
- Heating, ventilation and air-conditioning

2. Mechanical (MCAD) Engineering

- Automotive – Vehicles
- Aerospace
- Consumer goods
- Machinery
- Ship building
- Bio-mechanical system

3. Electronic Design Automation (EDA)

- Electronic and electrical (ECAD)
- Digital circuit design

4. Electrical Engineering

- Power systems engineering
- Power analytics

5. Manufacturing Process Planning

6. Industrial Design

7. Software Application

8. Apparel and Textile CAD

- Fashion design

9. Garden Design

The capabilities of modern CAD systems include:

- Wireframe geometry creation
- 3D parametric feature based modeling, solid modeling
- Freeform surface modeling
- Automated design of assemblies
- Create engineering drawings from the solid models
- Reuse of the design components
- Easy to modify the model of design and the production of multiple versions
- Automatic generation of standard components of the design
- Validation/verification of designs against specifications and design rules
- Simulation of designs without building a physical prototype
- Output of engineering documentation, such as manufacturing drawings, and BOM to reflect the requirement building the product
- Easy to exchange data within different software packages
- Provide design data directly to manufacturing facilities
- Output directly to a rapid prototyping or rapid manufacturing machine for industrial prototypes
- Maintain libraries of parts and assemblies
- Calculate mass properties of parts and assemblies
- Aid visualization with shading, rotating, hidden line removal, etc...
- Bi-directional parametric association (modification of any feature is reflected in all information relying on that feature: drawings, mass properties, assemblies, etc... and counter wise)
- Kinematics, interference and clearance checking of assemblies

- Sheet metal design
- Hose/cable routing
- Electrical component packaging
- Inclusion of programming code in a model to control and relate desired attributes of the model
- Programmable design studies and optimization
- Sophisticated visual analysis routines, for draft, curvature, curvature continuity.

1.1.4 Advantages of CAD

Today's industries cannot survive in the worldwide competition unless they introduce new products with better quality, at lower cost, and with shorter lead time. Accordingly, they have tried to use the computer's huge memory capacity, fast processing speed, and user-friendly interactive graphics capabilities to automate and tie together the cumbersome and separate engineering or production tasks. Thus this reduces the product cycle time and the cost of product development and production. CAD is one of the technologies tool used to serve this purpose during the product cycle.

CAD demonstrates its advantages compared with conventional design in the following areas based on its solid model:

- Reduction in design and product cycle time
- Convenience for design modification
- Convenient for die/mould design
- Convenient for FEM analysis
- Convenience for CNC programming
- Convenience for data storage
- Design in parametric method

1.2 Parametric Design

1.2.1 Definition of Parametric Design

When talking about CAD, we cannot neglect parametric design. Parametric design refers to using parameters to define relations which are actually in determining the design elements or features. The basis for the parametric design is a dimension-driven geometry, which means, in dimension-driven geometry, any changes in dimensions will generate changes in geometry. In parametric design, geometric elements of CAD models are connected with parameters. This approach may be used in explicit definition of the geometry of B-rep by replacing dimensions by variable parameters in implicit geometry definitions, such as Constructive Solid Geometry (CSG).

1.2.2 Parametric Design

Engineering design can be described as a set of decision-making processes and activities which is involved in determining the form of an object product. Parametric design is one of the phases in the development of a product, these phases including: formulation, concept design, configuration design, parametric design, and detail design. What makes parametric design special and particularly challenging is that analytical and experimental methods are employed to predict and evaluate the behaviour of each design object. Parametric design usually requires following four steps:

- Definition of a sketch
- Definition of geometric constraints between design elements
- Constraint solving
- Generation of variations by changing parameters

Most current CAD software chooses parametric method; in the past several years, Pro/E is the major CAD software which proves the success of parametric design and prompts other CAD provider to develop similar functions. A parameter is a variable to which other variables are related and by which these other variables can be obtained by means of equations defined. By this parametric manner, modification of design and creation of a family of parts can be performed in remarkably quick time compared with the redrawing required by non parametric design. Parametric design can be accomplished with a spreadsheet (or table sheet), script, or by manually changing dimension in the model. These characteristics can make fewer job-loads in the process of design and modification. For example, a family of parts, one of the important set in parametric design, which is

described in same shape and feature of parts but constrained in different dimensions and relations, can be easily established by parametric design method with one model defined by a table of different dimensions or constraints in CATIA.

It should be noted that, from an elementary view point, parametric design is widely used in industry to reduce the effort needed to change CAD model and to create design variants but there is no clear boundaries between what is called parametric design and what is called computer aided drafting or modeling since modern CAD software relies on parametric design method.

1.3 Area Moment of Inertia

The area moment of inertia is the second moment of area around a given axis. Its definition is $I_x = \int y^2 \cdot dA$, when the section is symmetrical about the x or y axis. When this is not the case, the area moment of inertia around the y axis, I_y , and the product moment of area, I_{xy} , are required to obtain different area moment of inertia around different axis. It is a property of a sectional shape that is used to measure the resistance to bending and deflection. The SI unit of the second moment of area is m^4 .

For accurate CNC machining, we need to calculate area moments of inertia of end-mills to predict machined errors and to simulate machined surfaces. Prediction accuracy and simulation results are depend on how accurate the moments of inertia are. Until now, the area moment of inertia of a cutting tool is still approximated as a cantilevered beam with

an effective radius as 80% of the radius of the cutting tool. But in an actual cutting tool, with different cutting flutes, the section of the cutting tool may not be a symmetrical shape. For example, a two-flute cutting tool is not a symmetrical one, but the other end-mills are. Their deflections caused by the cutting tool in a different axis direction are different.

1.4 Literature Review

Some published papers discussed about the generalized model for cutting tools, including mathematical and manufacturing models [1-9]. Engin, and Altintas [1] describe a generalized mathematical model of most helical end mills used in the industry. The end mill geometry is modeled by helical flutes wrapped around a parametric envelope and the helical curve of a cutting edge is mathematically expressed, which can be applied to the parametric design and representation of varieties of end mills. Chen, *et al.* [2] present a comprehensive manufacturing model that can be used to produce a concave cone-end milling cutter on a 2-axis NC machine. Based on the given design parameters and criteria, the equation of the cutting flute and the curve of the cutting edge are derived. Chen, *et al.* [3] present a method for manufacturing concave-arc ball-end cutters using a 2-axis NC machine. The models that are used to calculate the actually obtained flute and the computer simulation method are also introduced. Wang, *et al.* [4] present the geometrical and manufacturing models of the rake face and flank by introducing a sphere and helicoid model used to grind the rake face and flank of the cutter. Chen, *et al.* [5] develop a systematic method that integrates design, manufacturing, simulation, and

remedy. Based on the envelope condition, approaches for solving the direct and inverse problems related to the manufacturing models are also presented. Lin, *et al.* [6] present a mathematical model for a ball-end cutter that can be used to design and manufacture by using a 2-axis NC machine. Tsai, *et al.* [7] propose an analysis method that integrates design, manufacturing and numerical simulation to obtain a manufacturing model of the design and NC manufacturing of a ball-end cutter. Furthermore, a helical curve of the cutting edge, the equation of the sectional flute, and the mathematical model of the cross section of the grinding wheel, are also presented. Chen, *et al.* [8] present a mathematic model of the helical curve of the cutting edge and cutting flute, the design of the grinding wheels used in the NC machining of toroid-shaped cutters with a concave-arc generator. Chen, *et al.* [9] build mathematical models to overcome the two major problems associated with the design and manufacturing of ball-end cutters. The first problem involves the inability to solve the mathematical description of the cutting edge at the top of the ball-end cutter, while the second problem relates to the description of the grinding wheel feeding speed approaching infinity in the same region. All the 9 papers are focused on NC manufacturing model, the envelope model without sectional cutting flute model, more than the CAD parametric design model. No CAD models of the cutting flute on the ball or bull head is developed. Liu, *et al.* [10] study the design of hob cutters for generating the multi-cutting angles (radial rake angle, relief angle, and clearance angel) of helical cutting tools on one hobbing process. This paper discusses manufacturing processes with a hob instead of a grinding wheel.

Since this thesis is about CAD parametric design, some papers about CAD are reviewed [11-13]. Sheth, *et al.* [11], basically, present mathematical analysis for CAD/CAM

system for the design and manufacture of components with helical flutes. The CAD system can help the user design the profile of the tool and the helical flute, and thereafter analyze the subsequent machining process. Kaldor, *et al.* [12] deal with geometrical analysis and development for the designing of the cutter and the grinding wheel profile. The “direct” and the “indirect” method allow for the prediction of the helical flute profiles and cutter profiles, respectively. KANG, *et al.* [13] propose an analytical resolution of helical flute machining through a CAD approach, and a generalized helical flute machining model, utilizing the principles of differential geometry and kinematics, has been formulated. These 3 papers discuss CAD, but do not deal with building the cutter model. One paper on calculating rotary inertia is reviewed [14]. Rincon, *et al.* [14] present a transverse vibration model for drill bits which includes the effects of gyroscopic moments and rotary inertia. The model is used to demonstrate the significance of these effects, and of complex drill geometries, on the natural frequencies of drill bit transverse vibration. This paper discusses the rotary inertia of drill bits, but not the milling cutters.

1.5 Research Objectives

Due to cutting forces and the flexibility of the tool and its holder, the tool (or end-mill) deflects when it is engaging with the workpiece; unfortunately, large deflections can cost part accuracy, even break the tool. To produce high-precision parts, it is important to predict the deflections with high fidelity and then greatly reduce them through compensation in CNC tool paths. For this purpose, many research works have been successfully conducted on cutting forces prediction; however, another critical factor, the

area moment of inertia of the tool, is always approximated, significantly reducing the accuracy of estimated deflections. The main reason for this is that the 3-D geometric model of end-mills is difficult to construct. To find the moment of inertia, the objectives of this work are to establish a parametric model of APT cutters and implement in the CATIA CAD/CAM system by using its API, and to calculate the area moment of inertia for end-mills. This work can be used, together with an existing cutting force calculation method, to accurately predict cutter deflections during milling in order to compensate them in CNC tool paths. It can also provide more precise 3-D solid models of end-mills for machining simulation by using finite element analysis.

1.6 Thesis Outline

This thesis comprises of 7 chapters. Chapter one introduces some basic concepts of CAD, parametric design, area moment of inertia, literature review and thesis objectives. Chapter two and three presents the parametric representation of cutting edges and cutting flutes, respectively. Chapter four describes the calculation of the area moment of inertia based on the sectional flute model built in Chapter two and three. In Chapters five and six, some examples of cutting tool are presented and their area moment of inertia is calculated, the analysis of the difference of the area moment of inertia between the presented model and traditional way and some examples of the equivalent radius or calculated area moment of inertia is provided. Chapter seven describes the major work of this thesis and future work. In Chapter eight, some of the appendixes are introduced, which is applied by Chapter four.

Chapter 2 Parametric Representation of the Cutting Edges of APT Cutters

2.1 Nomenclature

α : The angle of the taper of an APT cutter

β : The angle of the conical surface at the APT cutter bottom

θ : The helical angle of the cutting edge of an APT cutter

R_s : The radial distance between the fillet center S and the cutter axis

r_c : The corner (fillet) radius of the cutter

l_1 : The axial length of the cutter taper

l_2 : The axial length of the cylindrical shank

l_3 : The axial length of the conical surface at the cutter bottom

n : Teeth (or flute) number of the cutter

γ_1 : Rake angle of the cutting edge

γ_2 : Relief (or clearance) angle of the cutting edge

γ_3 : Angle of straight line DE to X-axis (Clearance angle)

r_1 Radius of arc BC of flute

r_2 Radius of arc CD of flute

r_0 Radius of the annular land on the end cutting surface

l_{EF} Length of cutting edge strip EF

ϑ Parameter of the revolving surface

z_s Axial coordinate of the end mill

z_k Axial coordinate of the end mill

2.2 Parametric Representation of the Envelopes of APT Cutters

APT (or automatically programmed tool) milling cutters are in generic shape, which can represent the geometries of all end-mills used in industry. To build the solid models of end-mills for various purposes, an effective way is to conduct a parametric design of APT cutters, and then a specific end-mill model can be obtained by assigning its corresponding parametric values. Specifically, a parametric design of APT cutters includes the parametric formulations of the helical cutting edge and the flute profile. By sweeping the flute profile along the cutting edge, the cutter body, the complex shape of a cutter, can be generated, and, by adding the cylindrical shank, a solid model of a cutter is completed. In the beginning of this section, a brief introduction to APT cutters is provided.

With regard to the geometry of a generic APT cutter, its envelop of the helical cutting edge is shown in Fig. 2.1, together with all the geometric notations used in my research work. It can be seen from the schematic that this envelope includes a conic surface (between points J and K), a toroidal fillet (between points K and L), a taper (between points L and M), and a cylindrical shank surface (between points M and N) from bottom to top. Among these envelope surfaces, the fillet normally is tangent to the taper and the conic bottom surface, despite of non-tangency between them in some special cutters, which is not addressed in my research work. The cutting edge is a helix on the envelope with a constant angle between the tangents of the cutting edge and the envelope longitudinal curve. Due to variation of the surfaces geometries, the segments of the helix on the surfaces are different from each other, so are their parametric equations. Thus, in order to define the helical cutting edge, the envelope surfaces have to be formulated before hand.

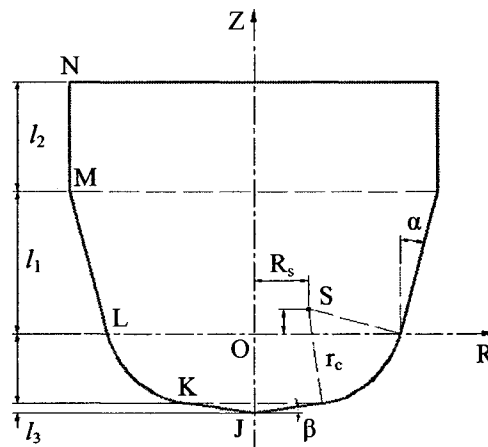


Figure 2-1 Schematic of the envelope of an APT cutter in the tool coordinate system.

The generalized parametric model can define a variety of end mills used in industry. These seven geometric parameters, $R_L, rc, R_S, zS, \alpha, \beta, l_1$, are independent of each other, but with geometric constraints to create mathematically realizable shape.

Flat End Mill	Ball End Mill	Bull Nose End Mill
$R_L \neq 0, rc = 0, R_S = R_L$ $zS = 0, \alpha = \beta = 0, l_1 \neq 0$	$R_L \neq 0, rc = R_L, R_S = 0$ $zS = 0, \alpha = \beta = 0, l_1 \neq 0$	$R_L \neq 0, rc \neq 0, R_S \neq 0$ $zS = 0, \alpha = \beta = 0, l_1 \neq 0$
Taper Flat End Mill	Taper Ball End Mill	General End Mill
$R_L \neq 0, rc = 0, R_S = R_L$ $zS = 0, \alpha = 0, \beta \neq 0, l_1 \neq 0$	$R_L \neq 0, rc = R_L, R_S = 0$ $zS = 0, \alpha = 0, \beta \neq 0, l_1 \neq 0$	$R_L \neq 0, rc \neq 0, R_S \neq 0$ $zS \neq 0, \alpha \neq 0, \beta \neq 0, l_1 \neq 0$
Cone End Mill	Rounded End Mill	Inverted Cone End Mill
$R_L \neq 0, rc = 0, R_S = R_L$ $zS = 0, \alpha \neq 0, \beta \neq 0, l_1 \neq 0$	$R_L \neq 0, rc \neq 0, R_S = 0$ $zS \neq 0, \alpha = \beta = 0, l_1 \neq 0$	$R_L \neq 0, rc \neq 0, R_S \neq 0$ $zS \neq 0, \alpha \neq 0, \beta \neq 0, l_1 \neq 0$

To derive parametric equations of all the envelop surfaces, a tool coordinate system (X-Y-Z) is first built for modeling the APT cutter shown in Fig. 2.1; the origin of the coordinate system is at point O, the Z-axis is directed upwards along the cutter axis, and the X- and Y-axes are on a plane perpendicular to the cutter axis. In this coordinate system, the parametric equations for different geometric shapes of the cutter envelope can be found in sequence, and the formulation details are provided in the following.

2.2.1 Parametric Equation of the Conic Surface

For generality, the conic surface of the envelope on the bottom of an APT cutter is taken into account in this work, even though many flat end-mills without the conic surface are used in industry. Since the conic surface forms a non-zero angle β with a horizontal plane, its radius at different height can be found as

$$R(z) = \frac{1}{\tan \beta} \cdot (z - z_J). \quad (2.1)$$

where $z_J = z_K - l_3$, $l_3 = R_K \cdot \tan \beta$, and

$$\begin{cases} R_K = R_s + r_c \cdot \sin \beta \\ z_K = z_s - r_c \cdot \cos \beta \end{cases}.$$

Thus, the parametric equation of the conic surface is

$$S_{JK}(z, \psi) = \begin{bmatrix} \frac{1}{\tan \beta} \cdot (z - z_J) \cdot \cos \psi \\ \frac{1}{\tan \beta} \cdot (z - z_J) \cdot \sin \psi \\ z \end{bmatrix}, \text{ and } \begin{pmatrix} z_J \leq z \leq z_K \\ 0 \leq \psi < 2 \cdot \pi \end{pmatrix}. \quad (2.2)$$

Where ψ is a parametric angle starting from the positive X-axis, and z is a parameter of the z coordinate.

2.2.2 Parametric Equation of the Fillet

The fillet of the envelope usually is the main portion of the cutter involved in stock material removing, and it is in toroidal shape. Since the radius of the circle on the fillet at a height can be computed with the equation

$$R(z) = R_s + \sqrt{r_c^2 - (z_s - z)^2}, \quad (2.3)$$

the fillet can be represented with parameters ψ and z as

$$\mathbf{S}_{KL}(z, \psi) = \begin{bmatrix} (R_s + \sqrt{r_c^2 - (z_s - z)^2}) \cdot \cos \psi \\ (R_s + \sqrt{r_c^2 - (z_s - z)^2}) \cdot \sin \psi \\ z \end{bmatrix}, \text{ and } \begin{pmatrix} z_k \leq z \leq 0 \\ 0 \leq \psi < 2\pi \end{pmatrix}. \quad (2.4)$$

2.2.3 Parametric Equation of the Taper

The taper shape of a cutter can increase its rigidity and reduce vibration during machining. In terms of a z coordinate, the radius of any cross-sectional circle of the taper is found as

$$R(z) = R_L + z \cdot \tan \alpha, \quad (2.5)$$

where $R_L = R_s + r_c \cdot \cos \alpha$. So, the taper equation in a parametric form is

$$\mathbf{S}_{LM}(z, \psi) = \begin{bmatrix} (R_L + z \cdot \tan \alpha) \cdot \cos \psi \\ (R_L + z \cdot \tan \alpha) \cdot \sin \psi \\ z \end{bmatrix}, \text{ and } \begin{pmatrix} 0 \leq z \leq l_1 \\ 0 \leq \psi < 2\pi \end{pmatrix}. \quad (2.6)$$

2.3 Parametric Representation of the Helical Cutting Edge

To build geometric models of APT cutters, a tooth's cutting edge, which is a helical curve, have to be formulated. According to a popular definition of helix in industry, a helical angle at a point is between the tangent to the helix and a plane through the cutter axis. Mathematically, helical cutting edges are on the envelope surfaces, and a helical angle is between the tangents to the cutting edge and the surface longitudinal curve (or line). Usually, helical angles remain constant and equal to the specified value. This general definition covers helical curves on different revolving surfaces such as cylinders, cones, and torus. For a helix on a cylinder, since the tangent to a longitudinal line is parallel to the tool axis, a helical angle is between the tangent to the curve and the cylinder axis, which is a convention. However, for helices on cones and torus, a helical angle at a point is not between the tangent to the curve and the cutter axis. Based on the parametric equations of the envelope surfaces, the formula of the tangents to the surfaces can be derived. Then, a differential equation of the helical segment on each envelope surface can be established, and this equation can be directly used to calculate points on the helical segment. By importing these points, the helical cutting edge can be plotted in CAD systems, such as the CATIA CAD/CAM system.

2.3.1 Helical Segment on the Conic Surface

A helical segment $P_{JK}(z)$ of the cutting edge on the bottom conic surface can be parameterized with its z coordinate; thus, each edge point can be represented as

$S_{JK}(z, \psi)$ with $\psi = \psi(z)$, where ψ is called a lag angle of the. Therefore, the equation of the helical segment, $P_{JK}(z)$, can be expressed as

$$P_{JK}(z) = \begin{bmatrix} x(z) \\ y(z) \\ z \end{bmatrix} = S_{JK}(z, \psi(z)) = \begin{bmatrix} \frac{1}{\tan \beta} \cdot (z - z_1) \cdot \cos \psi(z) \\ \frac{1}{\tan \beta} \cdot (z - z_1) \cdot \sin \psi(z) \\ z \end{bmatrix}. \quad (2.7)$$

The tangent vector of the helix can be found with the first derivative of $P_{JK}(z)$ in terms of z , which is

$$\frac{dP_{JK}}{dz} = \frac{dS_{JK}(z, \psi(z))}{dz} = \frac{\partial S_{JK}}{\partial z} + \frac{\partial S_{JK}}{\partial \psi} \cdot \frac{d\psi}{dz}. \quad (2.8)$$

Hence, the tangential vector dP_{JK} is found as the following equation.

$$dP_{JK}(z) = \frac{\partial S_{JK}}{\partial z} \cdot dz + \frac{\partial S_{JK}}{\partial \psi} \cdot d\psi. \quad (2.9)$$

According to the parametric equation of the conic surface above,

$$\frac{\partial S_{JK}}{\partial z} = \begin{bmatrix} \frac{1}{\tan \beta} \cdot \cos \psi \\ \frac{1}{\tan \beta} \cdot \sin \psi \\ 1 \end{bmatrix}, \quad (2.10)$$

and

$$\frac{\partial \mathbf{S}_{JK}}{\partial \psi} = \begin{bmatrix} \frac{-1}{\tan \beta} \cdot (z - z_J) \cdot \sin \psi \\ \frac{1}{\tan \beta} \cdot (z - z_J) \cdot \cos \psi \\ 0 \end{bmatrix}, \quad (2.11)$$

are obtained. Therefore, the tangent vector of the helical segment is

$$d\mathbf{P}_{JK}(z) = \frac{1}{\tan \beta} \cdot \begin{bmatrix} \cos \psi \cdot dz - (z - z_J) \cdot \sin \psi \cdot d\psi \\ \sin \psi \cdot dz + (z - z_J) \cdot \cos \psi \cdot d\psi \\ \tan \beta \cdot dz \end{bmatrix}, \quad (2.12)$$

and, the square of the module of the tangential vector, $d\mathbf{P}_{JK}(z)$ is

$$|d\mathbf{P}_{JK}|^2 = \frac{1}{\sin^2 \beta} \cdot \left((dz)^2 + (z_J - z)^2 \cdot \cos^2 \beta \cdot (d\psi)^2 \right). \quad (2.13)$$

A longitudinal line of the conic surface is a line on the surface, along which a point's parameter ψ is in-variant, independent of parameter z , so the parametric equation of a longitudinal line $\mathbf{Q}_{JK}(z)$ on this conic surface can be represented as

$$\mathbf{Q}_{JK}(z) = \begin{bmatrix} x(z) \\ y(z) \\ z \end{bmatrix} = \mathbf{S}_{JK}(z, \psi) = \begin{bmatrix} \frac{1}{\tan \beta} \cdot (z - z_J) \cdot \cos \psi \\ \frac{1}{\tan \beta} \cdot (z - z_J) \cdot \sin \psi \\ z \end{bmatrix}. \quad (2.14)$$

The tangent vector of the longitudinal line is the first derivative of $\mathbf{Q}_{JK}(z)$ in terms of z , which is

$$\frac{d\mathbf{Q}_{JK}}{dz} = \frac{d\mathbf{S}_{JK}(z, \psi)}{dz} = \frac{\partial \mathbf{S}_{JK}}{\partial z}. \quad (2.15)$$

So, the tangential vector $d\mathbf{Q}_{JK}$ of the longitudinal line is

$$d\mathbf{Q}_{JK}(z) = \frac{\partial \mathbf{S}_{JK}}{\partial z} \cdot dz = \begin{bmatrix} \frac{1}{\tan \beta} \cdot \cos \psi \cdot dz \\ \frac{1}{\tan \beta} \cdot \sin \psi \cdot dz \\ dz \end{bmatrix}. \quad (2.16)$$

The module of this tangential vector $d\mathbf{Q}_{JK}$ is

$$|d\mathbf{Q}_{JK}| = \frac{dz}{\sin \beta}, \quad (2.17)$$

due to β normally is about positive ten degrees. By referring to the helix definition, the helical angle θ is between the tangent vectors $d\mathbf{Q}_{JK}$ and $d\mathbf{P}_{JK}$, it can be expressed with the following equation.

$$\cos \theta = \frac{d\mathbf{P}_{JK} \cdot d\mathbf{Q}_{JK}}{|d\mathbf{P}_{JK}| \cdot |d\mathbf{Q}_{JK}|}, \quad (2.18)$$

By simplifying the above equation, we can get

$$\cos^2 \theta = \frac{(dz)^2}{(dz)^2 + (z_j - z)^2 \cdot \cos^2 \beta \cdot (d\psi)^2}, \quad (2.19)$$

thus, the relationship between lag angle ψ and dz of the helix is found in a differential form.

$$(d\psi)^2 = \left(\frac{\tan \theta}{\cos \beta \cdot (z_j - z)} \cdot dz \right)^2. \quad (2.20)$$

From Eq. (2.20), it is known that $d\psi$ can be positive or negative, which represents a right- or left-hand helix curve, respectively. For a right-hand helix curve cutting edge, the relationship between $d\psi$ and z at the cone zone can be found as

$$d\psi = \frac{\tan \theta}{\cos \beta} \cdot \frac{dz}{(z - z_j)}, \quad (2.21)$$

and, for a left hand helix curve cutting edge, the relationship between $d\psi$ and z at the cone zone can be built as

$$d\psi = -\frac{\tan \theta}{\cos \beta} \cdot \frac{dz}{(z - z_j)}. \quad (2.22)$$

2.3.2 Helical Segment on the Fillet

The helical curve $\mathbf{P}_{KL}(z)$ is on the torus surface with its helical lag angle ψ related with the parameter z , hence, the helix curve equation is

$$\mathbf{P}_{KL}(z) = \begin{bmatrix} x(z) \\ y(z) \\ z \end{bmatrix} = \mathbf{S}_{KL}(z, \psi(z)) = \begin{bmatrix} \left(R_s + \sqrt{r_c^2 - (z_s - z)^2} \right) \cdot \cos \psi(z) \\ \left(R_s + \sqrt{r_c^2 - (z_s - z)^2} \right) \cdot \sin \psi(z) \\ z \end{bmatrix}. \quad (2.23)$$

Since the first derivative of the helix is

$$\frac{d\mathbf{P}_{\text{KL}}}{dz} = \frac{d\mathbf{S}_{\text{KL}}(z, \psi(z))}{dz} = \frac{\partial \mathbf{S}_{\text{KL}}}{\partial z} + \frac{\partial \mathbf{S}_{\text{KL}}}{\partial \psi} \cdot \frac{d\psi}{dz}, \quad (2.24)$$

the tangential vector $d\mathbf{P}_{\text{KL}}$ of this curve is

$$d\mathbf{P}_{\text{KL}}(z) = \frac{\partial \mathbf{S}_{\text{KL}}}{\partial z} \cdot dz + \frac{\partial \mathbf{S}_{\text{KL}}}{\partial \psi} \cdot d\psi. \quad (2.25)$$

By substituting the following two equations,

$$\frac{\partial \mathbf{S}_{\text{KL}}}{\partial z} = \begin{bmatrix} \frac{z}{\sqrt{r_c^2 - (z_s - z)^2}} \cdot \cos \psi \\ \frac{z}{\sqrt{r_c^2 - (z_s - z)^2}} \cdot \sin \psi \\ 1 \end{bmatrix}, \quad (2.26)$$

and

$$\frac{\partial \mathbf{S}_{\text{KL}}}{\partial \psi} = \begin{bmatrix} -\left(R_s + \sqrt{r_c^2 - (z_s - z)^2}\right) \cdot \sin \psi \\ \left(R_s + \sqrt{r_c^2 - (z_s - z)^2}\right) \cdot \cos \psi \\ 0 \end{bmatrix}, \quad (2.27)$$

into Eq. (2.25), the tangential vector of the helix can be obtained.

$$d\mathbf{P}_{\text{KL}} = \begin{bmatrix} \frac{z}{\sqrt{r_c^2 - (z_s - z)^2}} \cdot \cos \psi \cdot dz - \left(R_s + \sqrt{r_c^2 - (z_s - z)^2}\right) \cdot \sin \psi \cdot d\psi \\ \frac{z}{\sqrt{r_c^2 - (z_s - z)^2}} \cdot \sin \psi \cdot dz + \left(R_s + \sqrt{r_c^2 - (z_s - z)^2}\right) \cdot \cos \psi \cdot d\psi \\ dz \end{bmatrix}. \quad (2.28)$$

Then, the square of the module of this tangential vector $d\mathbf{P}_{\text{KL}}$ can be calculated as

$$|d\mathbf{P}_{\text{KL}}|^2 = \frac{r_c^2 + 2 \cdot z \cdot z_s - z_s^2}{r_c^2 - (z_s - z)^2} \cdot (dz)^2 + \left(R_s + \sqrt{r_c^2 - (z_s - z)^2} \right)^2 \cdot (d\psi)^2. \quad (2.29)$$

The longitudinal curve $\mathbf{Q}_{\text{KL}}(z)$ is on the torus surface with angle ψ fixed, thus the curve can be derived from the surface as

$$\mathbf{Q}_{\text{KL}}(z) = \begin{bmatrix} x(z) \\ y(z) \\ z \end{bmatrix} = \mathbf{S}_{\text{KL}}(z, \psi) = \begin{bmatrix} \left(R_s + \sqrt{r_c^2 - (z_s - z)^2} \right) \cdot \cos \psi \\ \left(R_s + \sqrt{r_c^2 - (z_s - z)^2} \right) \cdot \sin \psi \\ z \end{bmatrix}. \quad (2.30)$$

Since the first derivative of the longitudinal curve is

$$\frac{d\mathbf{Q}_{\text{KL}}}{dz} = \frac{d\mathbf{S}_{\text{KL}}(z, \psi)}{dz} = \frac{\partial \mathbf{S}_{\text{KL}}}{\partial z}, \quad (2.31)$$

the tangential vector of the curve is

$$d\mathbf{Q}_{\text{KL}}(z) = \frac{\partial \mathbf{S}_{\text{KL}}}{\partial z} \cdot dz. \quad (2.32)$$

Therefore, the tangential vector can be simplified as

$$d\mathbf{Q}_{\text{KL}}(z) = \begin{bmatrix} \frac{z \cdot \cos \psi}{\sqrt{r_c^2 - (z_s - z)^2}} \cdot dz \\ \frac{z \cdot \sin \psi}{\sqrt{r_c^2 - (z_s - z)^2}} \cdot dz \\ dz \end{bmatrix}. \quad (2.33)$$

The module of the tangential vector $d\mathbf{Q}_{KL}$ is

$$|d\mathbf{Q}_{KL}| = \sqrt{\frac{z^2}{r_c^2 - (z_s - z)^2} + 1} \cdot dz, \quad (2.34)$$

The helical angle θ of the cutting edge is between tangents $d\mathbf{Q}_{KL}$ and $d\mathbf{P}_{KL}$, a equation of the helical angle is obtained.

$$\cos \theta = \frac{d\mathbf{Q}_{KL} \cdot d\mathbf{P}_{KL}}{|d\mathbf{Q}_{KL}| \cdot |d\mathbf{P}_{KL}|}. \quad (2.35)$$

Based on this equation, the relationship between the lag angle ψ and the z coordinate can be found.

$$(d\psi)^2 = \frac{(r_c^2 + 2 \cdot z \cdot z_s - z_s^2) \cdot \tan^2 \theta}{\left(R_s + \sqrt{r_c^2 - (z_s - z)^2}\right)^2 \cdot (r_c^2 - (z_s - z)^2)} \cdot (dz)^2. \quad (2.36)$$

It is easy to understand that $d\psi$ can be positive or negative to represent a right- or left-hand helical curve of the cutting edge, respectively. For a right-hand helical curve, the lag angle $d\psi$ can be calculated in terms of dz as

$$d\psi = \tan \theta \cdot \frac{\sqrt{r_c^2 + 2 \cdot z \cdot z_s - z_s^2}}{\left(R_s + \sqrt{r_c^2 - (z_s - z)^2}\right) \cdot \sqrt{r_c^2 - (z_s - z)^2}} \cdot dz, \quad (2.37)$$

and, for a left-hand cutting edge, the relationship between $d\psi$ and dz can be found as

$$d\psi = -\tan \theta \cdot \frac{\sqrt{r_c^2 + 2 \cdot z \cdot z_s - z_s^2}}{\left(R_s + \sqrt{r_c^2 - (z_s - z)^2}\right) \cdot \sqrt{r_c^2 - (z_s - z)^2}} \cdot dz. \quad (2.38)$$

2.3.3 Helical Segment on the Taper

The helical curve $\mathbf{P}_{LM}(z)$ is on the taper with the curve lag as a function of z , $\psi = \psi(z)$,

thus, the curve can be represented as

$$\mathbf{P}_{LM}(z) = \begin{bmatrix} x(z) \\ y(z) \\ z \end{bmatrix} = \mathbf{S}_{LM}(z, \psi) = \begin{bmatrix} (R_L + z \cdot \tan \alpha) \cdot \cos \psi \\ (R_L + z \cdot \tan \alpha) \cdot \sin \psi \\ z \end{bmatrix}. \quad (2.39)$$

Due to the first derivative of this helix,

$$\frac{d\mathbf{P}_{LM}}{dz} = \frac{d\mathbf{S}_{LM}(z, \psi)}{dz} = \frac{\partial \mathbf{S}_{LM}}{\partial z} + \frac{\partial \mathbf{S}_{LM}}{\partial \psi} \cdot \frac{d\psi}{dz}, \quad (2.40)$$

the tangential vector of this helix curve is

$$d\mathbf{P}_{LM}(z) = \frac{\partial \mathbf{S}_{LM}}{\partial z} \cdot dz + \frac{\partial \mathbf{S}_{LM}}{\partial \psi} \cdot d\psi, \quad (2.41)$$

By substituting the following equations

$$\frac{\partial \mathbf{S}_{LM}}{\partial z} = \begin{bmatrix} \tan \alpha \cdot \cos \psi \\ \tan \alpha \cdot \sin \psi \\ 1 \end{bmatrix}, \quad (2.42)$$

and

$$\frac{\partial \mathbf{S}_{LM}}{\partial \psi} = \begin{bmatrix} -(R_L + z \cdot \tan \alpha) \cdot \sin \psi \\ (R_L + z \cdot \tan \alpha) \cdot \cos \psi \\ 0 \end{bmatrix}, \quad (2.43)$$

into (2.41), the tangential vector of $\mathbf{P}_{LM}(z)$ can be found.

$$d\mathbf{P}_{LM} = \begin{bmatrix} \tan \alpha \cdot \cos \psi \cdot dz - (R_L + z \cdot \tan \alpha) \cdot \sin \psi \cdot d\psi \\ \tan \alpha \cdot \sin \psi \cdot dz + (R_L + z \cdot \tan \alpha) \cdot \cos \psi \cdot d\psi \\ dz \end{bmatrix}. \quad (2.44)$$

The module of the tangential vector $d\mathbf{P}_{LM}$ is

$$|d\mathbf{P}_{LM}|^2 = \left(\frac{dz}{\cos \alpha} \right)^2 + (R_L + z \cdot \tan \alpha)^2 \cdot (d\psi)^2. \quad (2.45)$$

Similar to the longitudinal lines on the conical surface, a longitudinal line $\mathbf{Q}_{LM}(z)$ on the taper can be found as

$$\mathbf{Q}_{LM}(z) = \begin{bmatrix} x(z) \\ y(z) \\ z \end{bmatrix} = \mathbf{S}_{LM}(z, \psi) = \begin{bmatrix} (R_L + z \cdot \tan \alpha) \cdot \cos \psi \\ (R_L + z \cdot \tan \alpha) \cdot \sin \psi \\ z \end{bmatrix}. \quad (2.46)$$

The first derivative of this longitudinal curve is

$$\frac{d\mathbf{Q}_{LM}}{dz} = \frac{d\mathbf{S}_{LM}(z, \psi)}{dz} = \frac{\partial \mathbf{S}_{LM}}{\partial z}, \quad (2.47)$$

so its tangential vector is

$$d\mathbf{Q}_{LM}(z) = \frac{\partial \mathbf{S}_{LM}}{\partial z} \cdot dz. \quad (2.48)$$

By simplification, the tangential vector is represented in the following equation.

$$d\mathbf{Q}_{LM} = \begin{bmatrix} \tan \alpha \cdot \cos \psi \cdot dz \\ \tan \alpha \cdot \sin \psi \cdot dz \\ dz \end{bmatrix}. \quad (2.49)$$

The module of the tangential vector $d\mathbf{Q}_{LM}$ can be found.

$$|d\mathbf{Q}_{LM}|^2 = \left(\frac{dz}{\cos \alpha} \right)^2. \quad (2.50)$$

The helical angle θ of the cutting edge is between tangents $d\mathbf{Q}_{LM}$ and $d\mathbf{P}_{LM}$, and can be formulated as

$$\cos \theta = \frac{d\mathbf{Q}_{LM} \cdot d\mathbf{P}_{LM}}{|d\mathbf{Q}_{LM}| \cdot |d\mathbf{P}_{LM}|}. \quad (2.51)$$

The lag angle of the helix can be calculated with the z coordinate in the following equation.

$$(d\psi)^2 = \tan^2 \theta \cdot \frac{(dz)^2}{\cos^2 \alpha \cdot (R_L + z \cdot \tan \alpha)^2}. \quad (2.52)$$

It is easy to understand that $d\psi$ can be positive or negative for a right- or left-hand, respectively. Thus, for a right-hand helix, the relationship between $d\psi$ and dz can be found as

$$d\psi = \tan \theta \cdot \frac{dz}{(R_L + z \cdot \tan \alpha) \cdot \cos \alpha}, \quad (2.53)$$

and, for a left-hand cutting edge, the relationship is as

$$d\psi = -\tan \theta \cdot \frac{dz}{(R_L + z \cdot \tan \alpha) \cdot \cos \alpha}. \quad (2.54)$$

In different zone, a series of representative equations of the differential helical lag angle have been established. Based on the equations, the helical lag angle can be calculated as

$$\psi_j(z) = \psi_{j-1}(z) + d\psi_j(z), \quad (2.55)$$

also, the radius of the section of the envelope of the cutting tool have been built, thus the helix curve can be calculated.

$$\begin{cases} x = r(z) \cdot \cos(\psi_j(z)) \\ y = r(z) \cdot \sin(\psi_j(z)) \\ z = z_j \end{cases} \quad (2.56)$$

2.4 Non Tangential Conditions

If cone zone JK is not tangential to arc zone KL at point K, then

$$R_K = R_S + \sqrt{r_c^2 - (z_S - z_K)^2}, \quad (2.57)$$

$$l_3 = R_K \cdot \tan \beta = \left(R_S + \sqrt{r_c^2 - (z_S - z_K)^2} \right) \cdot \tan \beta, \quad (2.58)$$

$$z_J = z_K - l_3; \quad (2.59)$$

if tapered zone LM is not tangential to arc zone KL at point L, then

$$\begin{cases} R_L = R_S + \sqrt{r_c^2 - z_S^2} \\ z_L = 0 \end{cases} \quad (2.60)$$

Chapter 3 Representation of Cutter Flutes

End-mills used in industry usually contain 2 to 4 teeth, between them are cutter flutes. The cross section of a cutter can be generated with a pattern of a flute profile, which is illustrated in Fig. 3.1, and the cutter teeth model can be formed by sweeping the cross section along the helical cutting edge. Each section of the flute consists of five segments. The straight line AB, which forms a rake angle γ_1 with the x axis, corresponds to the rake face. The circular arc BC with radius value r_1 is the section of the flute which blends the chip. The circular arc CD is the section of the flute which removes the chip smoothly. Let the radius of the arc CD be r_2 . Arc BC is tangent to the straight line AB at point B, and tangent to arc CD at point C. The straight line DE forms an angle γ_3 with the tangential line at point F. The straight line EF, which forms a relief angle γ_2 with the tangential line at point F, corresponds to the strip.

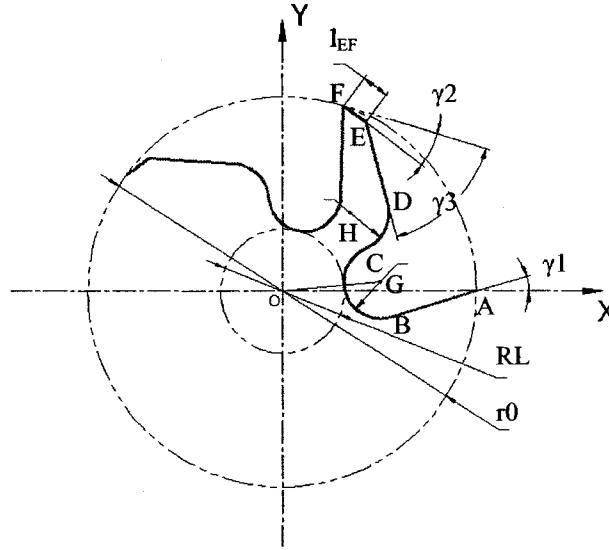


Figure 3-1 Sectional View of a Flute

3.1 The Coordinates of the Intersection Points of the Profile of Cutting Flute

Suppose an APT cutter has n teeth and the profile of a flute starts at point A (a tooth tip) on the X-axis and ends at point F (a neighboring tooth tip), as shown in Fig. 3.1. In this work, the central angle between two adjacent teeth is called a teeth spacing angle, which is shown in Fig. 3.1 as $\angle AOF$, and a teeth spacing angle is equal to $2\pi/n$. The x - and y -coordinates of points A and F can be found in the tool coordinate system.

$$\mathbf{r}_A = \begin{bmatrix} x_A \\ y_A \end{bmatrix} = \begin{bmatrix} R_L \\ 0 \end{bmatrix}, \quad (3.1)$$

and

$$\mathbf{r}_F = \begin{bmatrix} x_F \\ y_F \end{bmatrix} = \begin{bmatrix} R_L \cdot \cos\left(\frac{2\pi}{n}\right) \\ R_L \cdot \sin\left(\frac{2\pi}{n}\right) \end{bmatrix}. \quad (3.2)$$

The angle starting from the positive X-axis to line FE is denoted as ζ_{FE} , which can be found in terms of the relief angle γ_2 , teeth spacing angle, and helical cutting edge direction. For a right-hand helical cutting edge,

$$\zeta_{FE} = \frac{2\pi}{n} - \frac{\pi}{2} - \gamma_2, \quad (3.3)$$

and, for a left-hand helical cutting edge,

$$\zeta_{FE} = \frac{2\pi}{n} + \frac{\pi}{2} + \gamma_2. \quad (3.4)$$

According to point F, the coordinate of point E is calculated as

$$\begin{aligned} \mathbf{r}_E = \begin{bmatrix} x_E \\ y_E \end{bmatrix} &= \begin{bmatrix} x_F \\ y_F \end{bmatrix} + \begin{bmatrix} \cos \zeta_{FE} & -\sin \zeta_{FE} \\ \sin \zeta_{FE} & \cos \zeta_{FE} \end{bmatrix} \cdot \begin{bmatrix} l_{FE} \\ 0 \end{bmatrix} \\ &= \begin{bmatrix} x_F + l_{FE} \cdot \cos \zeta_{FE} \\ y_F + l_{FE} \cdot \sin \zeta_{FE} \end{bmatrix} \end{aligned} \quad (3.5)$$

The coordinates of point G can be represented in two ways, and then can be found by solving a system of equations.

$$\begin{aligned} \mathbf{r}_G &= [R_L - l_{AB} \cdot \cos \gamma_1 - r_1 \cdot \sin \gamma_1 \quad -l_{AB} \cdot \sin \gamma_1 + r_1 \cdot \cos \gamma_1] \\ &= [(r_1 + r_0) \cdot \cos \eta_1 \quad (r_1 + r_0) \cdot \sin \eta_1] \end{aligned} \quad (3.6)$$

which is

$$\begin{cases} R_L - l_{AB} \cdot \cos \gamma_1 - r_1 \cdot \sin \gamma_1 = (r_1 + r_0) \cdot \cos \eta_G \\ -l_{AB} \cdot \sin \gamma_1 + r_1 \cdot \cos \gamma_1 = (r_1 + r_0) \cdot \sin \eta_G \end{cases} \quad (3.7)$$

By solving this equation, l_{AB} and η_G are found as

$$\begin{cases} l_{AB} = \frac{-b_1 \pm \sqrt{b_1^2 - 4 \cdot a_1 \cdot c_1}}{2 \cdot a_1} \\ l_{AB} < R_L \\ \eta_G = \arcsin \left(\frac{r_1 \cdot \cos \gamma_1 - l_{AB} \cdot \sin \gamma_1}{r_1 + r_0} \right) \end{cases} \quad (3.8)$$

where

$$\begin{aligned} a_1 &= 1 \\ b_1 &= -2 \cdot R_L \cdot \cos \gamma_1 \\ c_1 &= R_L^2 - 2 \cdot R_L \cdot r_1 \cdot \sin \gamma_1 - r_0^2 - 2 \cdot r_0 \cdot r_1 \end{aligned} \quad (3.9)$$

Then, the coordinates of points B and G can be formulated as

$$\mathbf{r}_B = \begin{bmatrix} x_B \\ y_B \end{bmatrix} = \begin{bmatrix} x_A - l_{AB} \cdot \cos \gamma_1 \\ -l_{AB} \cdot \sin \gamma_1 \end{bmatrix}, \text{ and} \quad (3.10)$$

$$\mathbf{r}_G = \begin{bmatrix} x_G \\ y_G \end{bmatrix} = \begin{bmatrix} x_B - r_1 \cdot \sin \gamma_1 \\ y_B + r_1 \cdot \cos \gamma_1 \end{bmatrix}, \text{ respectively.} \quad (3.11)$$

Similarly, the angle starting from the positive X-axis to line ED is denoted as ζ_{ED} , and it can be formulated in terms of the clearance angle γ_3 , teeth spacing angle, and helical cutting edge direction. For a right-hand cutting edge,

$$\zeta_{ED} = \frac{2\pi}{n} - \frac{\pi}{2} - \gamma_3, \quad (3.12)$$

and, for a left-hand cutting edge,

$$\zeta_{ED} = \frac{2\pi}{n} + \frac{\pi}{2} + \gamma_3. \quad (3.13)$$

The coordinates of point H can be represented in two ways as in the following equation, with two unknown variables l_{ED} and η_2 .

$$\begin{aligned} \mathbf{r}_H &= \begin{bmatrix} x_E + l_{ED} \cdot \cos \zeta_{ED} - r_2 \cdot \cos \left(\frac{\pi}{2} + \zeta_{ED} \right) \\ y_E + l_{ED} \cdot \sin \zeta_{ED} - r_2 \cdot \sin \left(\frac{\pi}{2} + \zeta_{ED} \right) \end{bmatrix}, \\ &= \begin{bmatrix} x_G + (r_1 + r_2) \cdot \cos \eta_H \\ y_G + (r_1 + r_2) \cdot \sin \eta_H \end{bmatrix} \end{aligned} \quad (3.14)$$

which is a system of equations

$$\begin{cases} x_E + l_{ED} \cdot \cos \zeta_{ED} - r_2 \cdot \cos\left(\frac{\pi}{2} + \zeta_{ED}\right) = x_G + (r_1 + r_2) \cdot \cos \eta_H \\ y_E + l_{ED} \cdot \sin \zeta_{ED} - r_2 \cdot \sin\left(\frac{\pi}{2} + \zeta_{ED}\right) = y_G + (r_1 + r_2) \cdot \sin \eta_H \end{cases}, \quad (3.15)$$

By solving this equation, the variables l_{ED} and η_H are found.

$$\begin{cases} l_{ED} = \frac{-b_2 \pm \sqrt{b_2^2 - 4 \cdot a_2 \cdot c_2}}{2 \cdot a_2} \\ l_{ED} < R_L \cdot \frac{2\pi}{n} \\ \eta_H = \arcsin\left(\frac{y_E + l_{ED} \cdot \sin \zeta_{ED} - r_2 \cdot \cos \zeta_{ED} - y_G}{r_1 + r_2}\right) \end{cases}, \quad (3.16)$$

where

$$\begin{aligned} a_2 &= 1 \\ b_2 &= 2 \cdot \cos \zeta_{ED} \cdot (x_E - x_G + r_2 \cdot \sin \zeta_{ED}) + 2 \cdot \sin \zeta_{ED} \cdot (y_E - y_G - r_2 \cdot \cos \zeta_{ED}), \\ c_2 &= (x_E - x_G + r_2 \cdot \sin \zeta_{ED})^2 + (y_E - y_G - r_2 \cdot \cos \zeta_{ED})^2 - (r_1 + r_2)^2 \end{aligned} \quad (3.17)$$

Thus, the coordinates of points H, D, and C are calculated.

$$\mathbf{r}_H = \begin{bmatrix} x_H \\ y_H \end{bmatrix} = \begin{bmatrix} x_E + l_{ED} \cdot \cos \zeta_{ED} + r_2 \cdot \sin \zeta_{ED} \\ y_E + l_{ED} \cdot \sin \zeta_{ED} - r_2 \cdot \cos \zeta_{ED} \end{bmatrix}, \quad (3.18)$$

$$\mathbf{r}_D = \begin{bmatrix} x_D \\ y_D \end{bmatrix} = \begin{bmatrix} x_E + l_{ED} \cdot \cos \zeta_{ED} \\ y_E + l_{ED} \cdot \sin \zeta_{ED} \end{bmatrix}, \text{ and} \quad (3.19)$$

$$\mathbf{r}_C = \begin{bmatrix} x_C \\ y_C \end{bmatrix} = \begin{bmatrix} \frac{r_1 \cdot x_H + r_2 \cdot x_G}{r_1 + r_2} \\ \frac{r_1 \cdot y_H + r_2 \cdot y_G}{r_1 + r_2} \end{bmatrix}, \text{ respectively.} \quad (3.20)$$

3.2 Polar Equations of the Flute Segments

Based on the geometric feature points (A, B, C, D, E and F) of the flute found above, the flute profile including three lines (AB, ED, and FE) and two arcs (BC and CD), can be represented with polar equations. First, the polar representations for points A(ρ_A, η_A), B(ρ_B, η_B), C(ρ_C, η_C), D(ρ_D, η_D), E(ρ_E, η_E) and F(ρ_F, η_F) can be found as

$$\rho_A = R_L \text{ and } \eta_A = 0 \quad (3.21)$$

$$\rho_B = \sqrt{x_B^2 + y_B^2} \text{ and } \eta_B = \arctan\left(\frac{y_B}{x_B}\right), \quad (3.22)$$

$$\rho_C = \sqrt{x_C^2 + y_C^2} \text{ and } \eta_C = \arctan\left(\frac{y_C}{x_C}\right), \quad (3.23)$$

$$\rho_D = \sqrt{x_D^2 + y_D^2} \text{ and } \eta_D = \begin{cases} \pi + \arctan\left(\frac{y_D}{x_D}\right), & x_D < 0 \\ \arctan\left(\frac{y_D}{x_D}\right), & x_D \geq 0 \end{cases}, \quad (3.24)$$

$$\rho_E = \sqrt{x_E^2 + y_E^2} \text{ and } \eta_E = \begin{cases} \pi + \arctan\left(\frac{y_E}{x_E}\right), & x_E < 0 \\ \arctan\left(\frac{y_E}{x_E}\right), & x_E \geq 0 \end{cases}, \text{ and} \quad (3.25)$$

$$\rho_F = R_L \text{ and } \eta_F = \frac{2\pi}{n}. \quad (3.26)$$

For the centers G and H of arcs BC and CD, their polar coordinates representations

$G(\rho_G, \eta_G)$ and $H(\rho_H, \eta_H)$ can be calculated as

$$\rho_G = r_0 + r_1 \text{ and } \eta_G = \arctan\left(\frac{y_G}{x_G}\right), \quad (3.27)$$

and

$$\rho_H = \sqrt{x_H^2 + y_H^2}, \text{ and } \eta_H = \begin{cases} \pi + \arctan\left(\frac{y_H}{x_H}\right), & x_H < 0 \\ \arctan\left(\frac{y_H}{x_H}\right), & x_H \geq 0 \end{cases}, \quad (3.28)$$

respectively.

Second, polar equations of the flute segments are derived one by one. To derive a polar equation of line AB, the algebraic equation of this line in the Cartesian coordinate system is adopted.

$$y = \tan \gamma_1 \cdot (x - x_A) \quad (3.29)$$

Since the Cartesian coordinates (x, y) of a point on this line are co-related with the polar coordinates (ρ, η) of this point in an equation $\begin{cases} x = \rho \cdot \cos \eta \\ y = \rho \cdot \sin \eta \end{cases}$, by substituting the relationship, the above equation can be transformed into

$$\rho \cdot (\sin \gamma_1 \cdot \cos \eta - \cos \gamma_1 \cdot \sin \eta) = x_A \cdot \sin \gamma_1. \quad (3.30)$$

Hence, a polar equation of line AB is obtained after solving this equation.

$$\eta(\rho) = \gamma_1 - \arcsin\left(\frac{x_A \cdot \sin \gamma_1}{\rho}\right), \rho \in [\rho_A \quad \rho_B]. \quad (3.31)$$

For a polar equation of circular arc BC, based on the equation of arc BC in the Cartesian coordinate system, $(x - x_G)^2 + (y - y_G)^2 = r_1^2$, a equation of polar coordinates of this arc is obtained as

$$\rho^2 - 2 \cdot \rho \cdot \rho_G \cdot \cos(\eta - \eta_G) + \rho_G^2 = r_1^2. \quad (3.32)$$

By solving the above equation, a polar equation of arc BC is found as

$$\begin{cases} \eta_{BC}(\rho) = \eta_G + \arccos\left(\frac{\rho^2 + \rho_G^2 - r_1^2}{2 \cdot \rho \cdot \rho_G}\right), \rho \in [r_0 \quad \rho_C] \\ \eta_{BC}(\rho) = \eta_G - \arccos\left(\frac{\rho^2 + \rho_G^2 - r_1^2}{2 \cdot \rho \cdot \rho_G}\right), \rho \in [\rho_B \quad r_0] \end{cases}, \quad (3.33)$$

Similarly derived as circular arc BC, based on the equation of circular arc CD in the Cartesian coordinate system, $(x - x_H)^2 + (y - y_H)^2 = r_2^2$, a polar equation of circular arc CD is obtained as

$$\rho^2 - 2 \cdot \rho \cdot \rho_H \cdot \cos(\eta_{CD} - \eta_H) + \rho_H^2 = r_2^2. \quad (3.34)$$

By solving the above equation, we can build the polar equations of circular arc CD.

$$\begin{cases} \eta_{CD}(\rho) = \eta_H - \arccos\left(\frac{\rho^2 + \rho_H^2 - r_2^2}{2 \cdot \rho \cdot \rho_H}\right), \rho \in [\rho_C, \rho_H + r_2] \\ \eta_{CD}(\rho) = \eta_H + \arccos\left(\frac{\rho^2 + \rho_H^2 - r_2^2}{2 \cdot \rho \cdot \rho_H}\right), \rho \in [\rho_H + r_2, \rho_D] \end{cases}. \quad (3.35)$$

The function of the circular arc CD is the flute segment which removes the chips blended by circular arc BC smoothly. In practice design, $\eta_H > \eta_{CD}(\rho)$, that is,

$$\eta_{CD}(\rho) = \eta_H - \arccos\left(\frac{\rho^2 + \rho_H^2 - r_2^2}{2 \cdot \rho \cdot \rho_H}\right), \rho \in [\rho_C, \rho_H + r_2]. \quad (3.36)$$

To derive the polar equation of line DE, the relationship of a point coordinates between polar and Cartesian coordinate system is substituted into this line equation in the Cartesian coordinate system, $y = \tan \zeta_{DE} \cdot (x - x_D) + y_D$. This polar equation is found as

$$\rho \cdot (\sin \eta_{DE} \cdot \cos \zeta_{DE} - \cos \eta_{DE} \cdot \sin \zeta_{DE}) = y_D \cdot \cos \zeta_{DE} - x_D \cdot \sin \zeta_{DE}. \quad (3.37)$$

To find a representation polar equation by solving the above equation, we have

$$\eta_{DE}(\rho) = \arcsin\left(\frac{y_D \cdot \cos \zeta_{DE} - x_D \cdot \sin \zeta_{DE}}{\rho}\right) + \zeta_{DE}, \quad \rho \in [\rho_D \quad \rho_E]. \quad (3.38)$$

The steps and methods used to find a polar equation of line DE can be similarly applied to derive the polar equation of Line EF. Based on the algebraic equation of line EF in the Cartesian coordinate system, $y = \tan \zeta_{EF} \cdot (x - x_E) + y_E$, the polar equation of this line is founded.

$$\rho \cdot (\sin \eta_{EF} \cdot \cos \zeta_{EF} - \cos \eta_{EF} \cdot \sin \zeta_{EF}) = y_E \cdot \cos \zeta_{EF} - x_E \cdot \sin \zeta_{EF}. \quad (3.39)$$

Solving the above equation, a polar equation of this line is established.

$$\eta_{EF}(\rho) = \arcsin\left(\frac{y_E \cdot \cos \zeta_{EF} - x_E \cdot \sin \zeta_{EF}}{\rho}\right) + \zeta_{EF}, \quad \rho \in [\rho_E \quad \rho_F]. \quad (3.40)$$

For different section, the size of the sectional flute profile is scaled due to sectional radius. When the two end points of this profile are aligned to the helical lag angle along the helix curve, the profile of the flute can be built.

$$\begin{cases} \rho_j = S_j \cdot \rho \\ \eta_j = \eta(\rho) + \psi_j, \\ z_{fj} = z_j \end{cases} \quad (3.41)$$

and the scale, S_j , can be decided.

$$S_j = R(z) / R_L . \quad (3.42)$$

3.3 Program and the 3D Models of Cutting Tools

Based on the equations of helix cutting edges and the cutting flute profile built in chapter 2 and 3, parametric design in CAD of cutting tool can be done. By keying in the values of the parameters and clicking “Run” button shown in the bottom of Fig. 3.2, this program will run in CATIA V5 and 3D models of the cutting tools will be automatically produced.

Since the transitional section between cutting edges and shank is unpredictable, and it is decided by the shape of grinding wheel, the shape of the transition in the cutting tool is obtained by approximation.

Number of Flute	4	Corner Angle	15
Radius of Top Circle at Helical Section	12	Rounded Angle	15
Radius of Arc BC	4	Tapered Length	20
Radius of Arc CD	10	Corner Radius	4.14110472164
Radius of End Circle	6	Circle of Corner Radius R1	0
Length of EF	1	Circle of Corner Radius R2	1.037123629372
Flute Angle	35	Hole Angle	30
Flute Angle	5	Flank Length	15
Clearance Angle	45	Shank Length	60

Run

Figure 3-2 Parameters Interface.

Parameters on the left side of Fig. 3.2 are employed to describe the sectional cutting profile; and, parameters on the right side of Fig. 3.2 are used to describe the helix curve.

The following pictures show the solid model of several cutters produced by this program. They are flat end mill, ball nose end mill, bull nose end mill and Apt cutting tool, which are the representatives of the cutting tools that are being frequently used in manufacturing industrial. For some special designed cutting tools, the mathematical model also can be employed. But they are not the representatives of the popular ones in industrial, only for special application purposes.

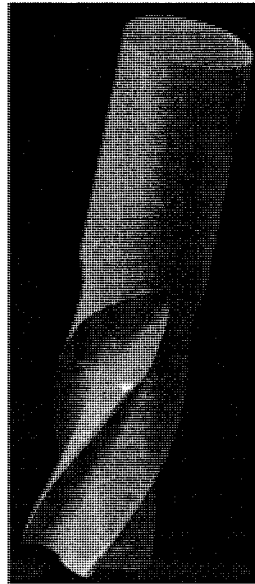


Figure 3-3 Flat End Mill

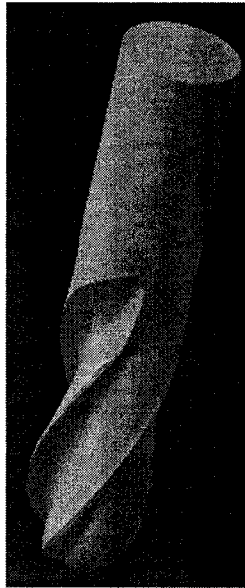


Figure 3-4 Ball Nose End Mill

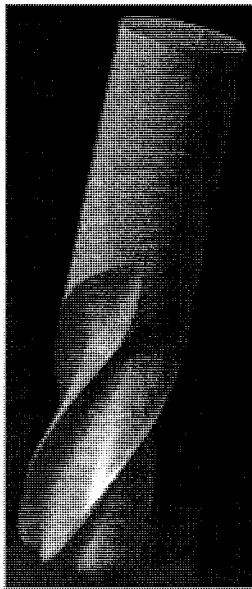


Figure 3-5 Bull Nosed End Mill



Figure 3-6 Apt Cutting Tool

Chapter 4 Accurate Calculation of Area Moments of Inertia of APT Cutters

Increasing demand for better quality products and higher production rates requires a more complete understanding of the inertia of cutting tools. When predicting machining error, the area moment of inertia is one of the very significant effects in calculating deflection [16]. If the I_x and I_y are not accurate enough, the calculated result of the deflection will not be accurate enough either. In this chapter, a more accurate method for calculating the area moment of inertia will be introduced.

In calculating the area moment of inertia, the cutting flute is considered as infinitesimal bands with the width, ΔR , and each infinitesimal band is divided into infinitesimal elements with an infinitesimal angle, $d\eta$. By calculating all the area moment of inertia of these infinitesimal areas and adding them together to obtain the area moment of inertia of bands, area moment of inertia of flute is obtained. The demonstration is shown in Fig. 3.1, and this layer is taken as a reference one at $z = 0$.

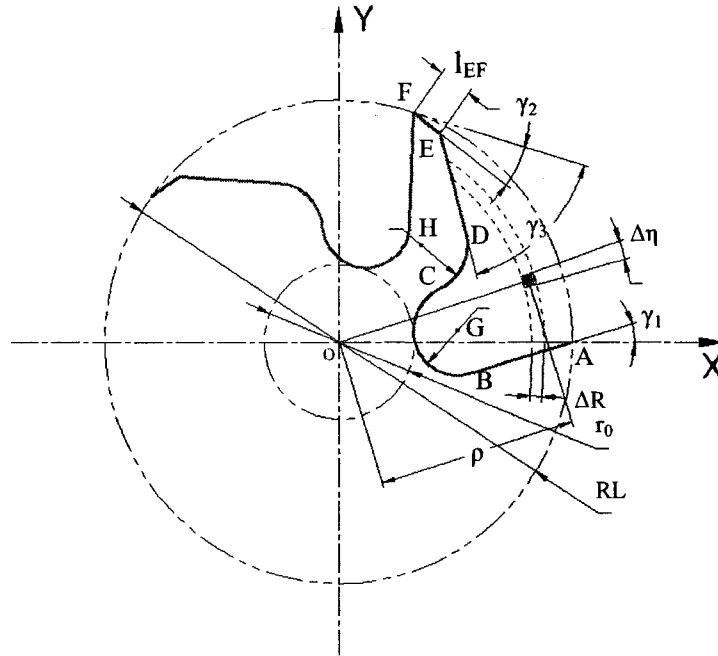


Figure 4-1 Diagram of one of the cutter flute.

4.1 Representation of Polar Angle

If the range of the polar radius between r_0 and R_L is divided into 1000 sections, then we can calculate the increment of polar radius and middle polar radii for bands.

$$nr = 1000,$$

$$\Delta R = \frac{R_L - r_0}{nr},$$

$$l = 1 : nr,$$

$$\rho = r_0 + (l - 0.5) \cdot \Delta R.$$

Concerning the profile of one cutter flute, as polar radius changes, the polar angle of each point on the curve of this profile will be represented in different formula. All these formula would be deduced in this section regarding to the profile of Fig. 3.1.

4.2 Difference of Polar Angle between Segments of Sectional Flute

Based on the design practice, the five equations of the five segments which consist of cutter flute and the intersectional points between segments would be different. Considering the relationship among ρ_B , ρ_C and ρ_D , three situations are established as polar radius changes from r_0 to R_L .

4.2.1 If $\rho_C \leq \rho_D \leq \rho_B$

If $r_0 \leq \rho \leq \rho_C$, this ρ range covers circular arc BC only

$$\Delta\eta(\rho) = \eta_{BC}^+(\rho) - \eta_{BC}^-(\rho) = 2 \cdot \arccos\left(\frac{\rho^2 + \rho_G^2 - r_1^2}{2 \cdot \rho \cdot \rho_G}\right), \quad (3.43)$$

if $\rho_C \leq \rho \leq \rho_D$, this range is surrounded by circular arcs CD and BC

$$\begin{aligned} \Delta\eta(\rho) &= \eta_{CD}(\rho) - \eta_{BC}^-(\rho) \\ &= \eta_H - \eta_G - \arccos\left(\frac{\rho^2 + \rho_H^2 - r_2^2}{2 \cdot \rho \cdot \rho_H}\right) + \arccos\left(\frac{\rho^2 + \rho_G^2 - r_1^2}{2 \cdot \rho \cdot \rho_G}\right), \end{aligned} \quad (3.44)$$

if $\rho_D \leq \rho \leq \rho_B$, this range is covered by line DE and circular arc BC

$$\begin{aligned}\Delta\eta(\rho) &= \eta_{DE}(\rho) - \eta_{BC}^-(\rho) \\ &= \arcsin\left(\frac{y_D \cdot \cos \zeta_{DE} - x_D \cdot \sin \zeta_{DE}}{\rho}\right), \\ &\quad + \zeta_{DE} - \eta_G + \arccos\left(\frac{\rho^2 + \rho_G^2 - r_1^2}{2 \cdot \rho \cdot \rho_G}\right)\end{aligned}\tag{3.45}$$

if $\rho_B \leq \rho \leq \rho_E$, this range is surrounded by lines DE and AB

$$\begin{aligned}\Delta\eta(\rho) &= \eta_{DE}(\rho) - \eta_{AB}(\rho) \\ &= \arcsin\left(\frac{y_D \cdot \cos \zeta_{DE} - x_D \cdot \sin \zeta_{DE}}{\rho}\right), \\ &\quad + \eta_{DE} - \gamma_1 + \arcsin\left(\frac{x_A \cdot \sin \gamma_1}{\rho}\right)\end{aligned}\tag{3.46}$$

if $\rho_E \leq \rho \leq \rho_F$, the two lines EF and AB form this range

$$\begin{aligned}\Delta\eta(\rho) &= \eta_{EF}(\rho) - \eta_{AB}(\rho) \\ &= \arcsin\left(\frac{y_E \cdot \cos \zeta_{EF} - x_E \cdot \sin \zeta_{EF}}{\rho}\right), \\ &\quad + \zeta_{EF} - \gamma_1 + \arcsin\left(\frac{x_A \cdot \sin \gamma_1}{\rho}\right)\end{aligned}\tag{3.47}$$

4.2.2 If $\rho_C \leq \rho_B \leq \rho_D$

If $r_0 \leq \rho \leq \rho_C$, this range includes circular arc BC only

$$\Delta\eta(\rho) = \eta_{AB}^+(\rho) - \eta_{AB}^-(\rho) = 2 \cdot \arccos\left(\frac{\rho^2 + \rho_G^2 - r_1^2}{2 \cdot \rho \cdot \rho_G}\right), \quad (3.48)$$

if $\rho_C \leq \rho \leq \rho_B$, this polar radius covers two circular arcs CD and BC

$$\begin{aligned} \Delta\eta(\rho) &= \eta_{CD}(\rho) - \eta_{AB}^-(\rho) \\ &= \eta_H - \eta_G - \arccos\left(\frac{\rho^2 + \rho_H^2 - r_2^2}{2 \cdot \rho \cdot \rho_H}\right) + \arccos\left(\frac{\rho^2 + \rho_G^2 - r_1^2}{2 \cdot \rho \cdot \rho_G}\right), \end{aligned} \quad (3.49)$$

if $\rho_B \leq \rho \leq \rho_D$, this range is covered by circular arc CD and line AB

$$\begin{aligned} \Delta\eta(\rho) &= \eta_{CD}(\rho) - \eta_{AB}(\rho) \\ &= \eta_H - \gamma_1 - \arccos\left(\frac{\rho^2 + \rho_H^2 - r_2^2}{2 \cdot \rho \cdot \rho_H}\right) + \arcsin\left(\frac{x_A \cdot \sin \gamma_1}{\rho}\right), \end{aligned} \quad (3.50)$$

if $\rho_D \leq \rho \leq \rho_E$, this range is covered by the two lines DE and AB

$$\begin{aligned} \Delta\eta(\rho) &= \eta_{DE}(\rho) - \eta_{AB}(\rho) \\ &= \arcsin\left(\frac{y_D \cdot \cos \zeta_{DE} - x_D \cdot \sin \zeta_{DE}}{\rho}\right) \\ &\quad + \zeta_{DE} - \gamma_1 + \arcsin\left(\frac{x_A \cdot \sin \gamma_1}{\rho}\right) \end{aligned} \quad (3.51)$$

if $\rho_E \leq \rho \leq \rho_F$, this range is surrounded by two lines EF and AB

$$\begin{aligned} \Delta\eta(\rho) &= \eta_{EF}(\rho) - \eta_{AB}(\rho) \\ &= \arcsin\left(\frac{y_E \cdot \cos \zeta_{EF} - x_E \cdot \sin \zeta_{EF}}{\rho}\right) \\ &\quad + \zeta_{EF} - \gamma_1 + \arcsin\left(\frac{x_A \cdot \sin \gamma_1}{\rho}\right) \end{aligned} \quad (3.52)$$

4.2.3 If $\rho_B \leq \rho_C \leq \rho_D$

If $r_0 \leq \rho \leq \rho_B$, in the range of arc BC only

$$\Delta\eta(\rho) = \eta_{BC}^+(\rho) - \eta_{BC}^-(\rho) = 2 \cdot \arccos\left(\frac{\rho^2 + \rho_G^2 - r_1^2}{2 \cdot \rho \cdot \rho_G}\right), \quad (3.53)$$

if $\rho_B \leq \rho \leq \rho_C$, in the area between circular arc BC and line AB

$$\begin{aligned} \Delta\eta(\rho) &= \eta_{BC}^+(\rho) - \eta_{AB}(\rho) \\ &= \eta_G - \gamma_1 + \arccos\left(\frac{\rho^2 + \rho_G^2 - r_1^2}{2 \cdot \rho \cdot \rho_G}\right) + \arcsin\left(\frac{x_A \cdot \sin \gamma_1}{\rho}\right), \end{aligned} \quad (3.54)$$

if $\rho_C \leq \rho \leq \rho_D$, in the area between circular arc CD and line AB

$$\begin{aligned} \Delta\eta(\rho) &= \eta_{CD}(\rho) - \eta_{AB}(\rho) \\ &= \eta_H - \gamma_1 - \arccos\left(\frac{\rho^2 + \rho_H^2 - r_2^2}{2 \cdot \rho \cdot \rho_H}\right) + \arcsin\left(\frac{x_A \cdot \sin \gamma_1}{\rho}\right), \end{aligned} \quad (3.55)$$

if $\rho_D \leq \rho \leq \rho_E$, in the area between tow lines DE and AB

$$\begin{aligned} \Delta\eta(\rho) &= \eta_{DE}(\rho) - \eta_{AB}(\rho) \\ &= \arcsin\left(\frac{y_D \cdot \cos \zeta_{DE} - x_D \cdot \sin \zeta_{DE}}{\rho}\right) \\ &\quad + \zeta_{DE} - \gamma_1 + \arcsin\left(\frac{x_A \cdot \sin \gamma_1}{\rho}\right) \end{aligned} \quad (3.56)$$

if $\rho_E \leq \rho \leq \rho_F$, in the area between two lines EF and AB

$$\begin{aligned}
\Delta\eta(\rho) &= \eta_{\text{EF}}(\rho) - \eta_{\text{AB}}(\rho) \\
&= \arcsin\left(\frac{y_{\text{E}} \cdot \cos \zeta_{\text{EF}} - x_{\text{E}} \cdot \sin \zeta_{\text{EF}}}{\rho}\right) \\
&\quad + \zeta_{\text{EF}} - \gamma_1 + \arcsin\left(\frac{x_{\text{A}} \cdot \sin \gamma_1}{\rho}\right)
\end{aligned} \tag{3.57}$$

The area moment of inertial of the first flute can be calculated based on the equations developed. By considering an area covered by $\Delta\eta(\rho)$ and ΔR as a band and in each band, $\Delta\eta(\rho)$ is divided into 100 elements, denoted as $d\eta(\rho)$.

$$\text{na} = 100,$$

$$d\eta(\rho) = \frac{\Delta\eta(\rho)}{\text{na}},$$

$$m = 1 : \text{na},$$

$$dA = \rho \cdot d\eta(\rho) \cdot \Delta R.$$

The area moment of inertia of each element around the x axis of each element is

if $\rho(l) \leq \rho_{\text{B}}$

$$\begin{aligned}
dI_x^m &= y^2 \cdot dA = \left(\rho \cdot \sin(\eta_{\text{BC}}^-(\rho) + (m-0.5) \cdot d\eta(\rho)) \right)^2 \cdot dA \\
&= \rho^3 \cdot \sin^2 \left(\left(\eta_{\text{BC}}^-(\rho) + (m-0.5) \cdot d\eta(\rho) \right) \right) \cdot d\eta(\rho) \cdot \Delta R,
\end{aligned} \tag{3.58}$$

else

$$\begin{aligned} dI_x^m &= y^2 \cdot dA = \left(\rho \cdot \sin(\eta_{AB}(\rho) + (m-0.5) \cdot d\eta(\rho)) \right)^2 \cdot dA \\ &= \rho^3 \cdot \sin^2 \left(\left(\eta_{AB}(\rho) + (m-0.5) \cdot d\eta(\rho) \right) \right) \cdot d\eta(\rho) \cdot \Delta R \end{aligned} \quad (3.59)$$

By adding all the area moment of inertia around the x axis of each element, the area moment of one certain band around the x axis is calculated.

$$\Delta I_x^l = \sum_{m=1}^{na} dI_x^m. \quad (3.60)$$

By adding all the area moment of inertia around the x axis of each band, the area moment of inertia around the x axis of first flute is obtained.

$$I_{fl_x}^l = \sum_{l=1}^{nr} \Delta I_x^l. \quad (3.61)$$

The area moment of inertia of each element around the y axis of each element is

if $\rho(l) \leq \rho_B$

$$\begin{aligned} dI_y^m &= x^2 \cdot dA = \left(\rho \cdot \cos(\eta_{BC}^-(\rho) + (m-0.5) \cdot d\eta(\rho)) \right)^2 \cdot dA \\ &= \rho^3 \cdot \cos^2 \left(\left(\eta_{BC}^-(\rho) + (m-0.5) \cdot d\eta(\rho) \right) \right) \cdot d\eta(\rho) \cdot \Delta R \end{aligned} \quad (3.62)$$

else

$$\begin{aligned}
dI_y^m &= x^2 \cdot dA = \left(\rho \cdot \cos(\eta_{AB}(\rho) + (m-0.5) \cdot d\eta(\rho)) \right)^2 \cdot dA \\
&= \rho^3 \cdot \cos^2 \left(\left(\eta_{AB}(\rho) + (m-0.5) \cdot d\eta(\rho) \right) \right) \cdot d\eta(\rho) \cdot \Delta R
\end{aligned} \tag{3.63}$$

The area moment of inertia around the y axis of one certain band is obtained by adding all the area moment of inertia around the y axis of each element,

$$\Delta I_y^l = \sum_{m=1}^{na} dI_y^m, \tag{3.64}$$

The area moment of inertia around the y axis of the first flute is calculated.

$$I_{\Omega,y}^l = \sum_{l=1}^{nr} \Delta I_y^l. \tag{3.65}$$

The product moment of area of each element is,

if $\rho(l) \leq \rho_B$

$$\begin{aligned}
dI_{xy}^m &= x \cdot y \cdot dA \\
&= \rho \cdot \cos \left(\left(\eta_{BC}^-(\rho) + (m-0.5) \cdot d\eta(\rho) \right) \right) \\
&\quad \cdot \rho \cdot \sin \left(\left(\eta_{BC}^-(\rho) + (m-0.5) \cdot d\eta(\rho) \right) \right) \cdot dA, \\
&= \rho^3 \cdot \cos \left(\left(\eta_{BC}^-(\rho) + (m-0.5) \cdot d\eta(\rho) \right) \right) \\
&\quad \cdot \sin \left(\left(\eta_{BC}^-(\rho) + (m-0.5) \cdot d\eta(\rho) \right) \right) \cdot d\eta(\rho) \cdot \Delta R
\end{aligned} \tag{3.66}$$

else

$$\begin{aligned}
dI_{xy}^m &= x \cdot y \cdot dA \\
&= \rho \cdot \cos\left(\left(\eta_{AB}(\rho) + (m-0.5) \cdot d\eta(\rho)\right)\right) \\
&\quad \cdot \rho \cdot \sin\left(\left(\eta_{AB}(\rho) + (m-0.5) \cdot d\eta(\rho)\right)\right) \cdot dA \quad . \quad (3.67) \\
&= \rho^3 \cdot \cos\left(\left(\eta_{AB}(\rho) + (m-0.5) \cdot d\eta(\rho)\right)\right) \\
&\quad \cdot \sin\left(\left(\eta_{AB}(\rho) + (m-0.5) \cdot d\eta(\rho)\right)\right) \cdot d\eta(\rho) \cdot \Delta R
\end{aligned}$$

For the product moment of area of one certain band, by adding all the product moment of area of each element together, the product moment of area of one band is obtained,

$$\Delta I_{xy}^l = \sum_{m=1}^{na} dI_{xy}^m, \quad (3.68)$$

By adding all product moment of area of each band, we can have the product moment of area of the first flute.

$$I_{\text{fl}_xy}^1 = \sum_{l=1}^{nr} \Delta I_{xy}^l. \quad (3.69)$$

Supposed the cutter has n flutes, thus, the area moment of inertia of each flute can be calculated by rotating an angle, $2\pi/n$, from its previous one. Then, according to the theorem by Benham [1] in his *Mechanics of solids and structures*, the area moment of inertia and the product moment of area for a coordinate system rotated relative to the original coordinate system can be calculated [Appendix I]. Applying to the cutter flute case, the other area moment of inertia and product moment of area of each flute is obtained.

$$I_{\text{flt}_x}^i = \frac{I_{\text{flt}_x}^{i-1} + I_{\text{flt}_y}^{i-1}}{2} + \frac{I_{\text{flt}_x}^{i-1} - I_{\text{flt}_y}^{i-1}}{2} \cdot \cos\left(2 \cdot \frac{2\pi}{n}\right) + I_{\text{flt}_{xy}}^{i-1} \cdot \sin\left(2 \cdot \frac{2\pi}{n}\right), \quad (3.70)$$

$$I_{\text{flt}_x}^i = \frac{I_{\text{flt}_x}^{i-1} + I_{\text{flt}_y}^{i-1}}{2} - \frac{I_{\text{flt}_x}^{i-1} - I_{\text{flt}_y}^{i-1}}{2} \cdot \cos\left(2 \cdot \frac{2\pi}{n}\right) - I_{\text{flt}_{xy}}^{i-1} \cdot \sin\left(2 \cdot \frac{2\pi}{n}\right), \quad (3.71)$$

$$I_{\text{flt}_{xy}}^i = -\frac{I_{\text{flt}_x}^{i-1} - I_{\text{flt}_y}^{i-1}}{2} \cdot \sin\left(2 \cdot \frac{2\pi}{n}\right) + I_{\text{flt}_{xy}}^{i-1} \cdot \cos\left(2 \cdot \frac{2\pi}{n}\right), \quad (3.72)$$

$$I_{\text{flt}_x}^n = \sum_{i=1}^n I_{\text{flt}_x}^i, \quad (3.73)$$

$$I_{\text{flt}_y}^n = \sum_{i=1}^n I_{\text{flt}_y}^i, \quad (3.74)$$

$$I_{\text{flt}_{xy}}^n = \sum_{i=1}^n I_{\text{flt}_{xy}}^i. \quad (3.75)$$

Thus the area moment of inertia of the cutter can be calculated.

$$I_{\text{ctr}_x} = \frac{\pi \cdot R_L^4}{4} - I_{\text{flt}_x}^n, \quad (3.76)$$

$$I_{\text{ctr}_y} = \frac{\pi \cdot R_L^4}{4} - I_{\text{flt}_y}^n, \quad (3.77)$$

$$I_{\text{ctr}_{xy}} = 0 - I_{\text{flt}_{xy}}^n. \quad (3.78)$$

If dividing the cutting tool into layers along the tool axis, which has a layer thickness dz , for different layer, the area moment of inertia would be different due to the lag angle of

helix curve shape cutting edges. The area moment of inertia of different layer can be calculated by rotating the reference one an helix angle, ψ_j .

$$^j I_{\text{ctr}_x} = S_j^4 \cdot \left(\frac{I_{\text{ctr}_x} + I_{\text{ctr}_y}}{2} + \frac{I_{\text{ctr}_x} - I_{\text{ctr}_y}}{2} \cdot \cos(2 \cdot \psi_j) + I_{\text{ctr}_{xy}} \cdot \sin(2 \cdot \psi_j) \right), \quad (3.79)$$

$$^j I_{\text{ctr}_y} = S_j^4 \cdot \left(\frac{I_{\text{ctr}_x} + I_{\text{ctr}_y}}{2} - \frac{I_{\text{ctr}_x} - I_{\text{ctr}_y}}{2} \cdot \cos(2 \cdot \psi_j) - I_{\text{ctr}_{xy}} \cdot \sin(2 \cdot \psi_j) \right), \quad (3.80)$$

$$^j I_{\text{ctr}_{xy}} = S_j^4 \cdot \left(-\frac{I_{\text{ctr}_x} - I_{\text{ctr}_y}}{2} \cdot \sin(2 \cdot \psi_j) + I_{\text{ctr}_{xy}} \cdot \cos(2 \cdot \psi_j) \right). \quad (3.81)$$

Chapter 5 Analysis and Comparison

5.1 Introduction

The cutting flutes of an end-mill significantly affect its area moment of inertia; however, this was covered by a traditional method. To highlight the difference of the moment of inertia by using this new and the traditional methods, the area moments of inertia of several cutting tools with a different number of flutes will be calculated and the results will be compared. In the examples, the design parameters such as the rake, relief, and clearance angles, of the cutting tool are the same, except for the number of flutes.

5.2 Influence of the Cutting Flutes

Table 5.1 shows the data of flat end-mills with different diameters. The seven parameters from column 4 to 10 are the same for the same diameter. Column 3 shows the number of flutes and column 2 is the diameter. The traditional method of calculating the moments of inertia is used by computing an effective cutting diameter, that is $R_e = 0.8 \cdot R_c$. It is evident that results of the traditional and new methods are quite different.

Table 5-1 Area of Moment of Inertia of Different End-Mills

Parameters of Cutting Flute									Moment of Inertia (mm ⁴)			Effect Radius	Equivalent Radius
Dia. (mm)	Flute No.	r ₀	r ₁	r ₂	l _{EF}	γ ₁	γ ₂	γ ₃	Traditional	New			
										I _x	I _y		
6	2	1.8	0.6	2.5	0.25	6	6	45	26.06	10.58	19.89	4.8	
	3								26.06	19.61	19.61		4.47
	4								26.06	22.06	22.06		4.60
	5								26.06	23.53	23.53		4.68
	6								26.06	24.10	24.10		4.71
8	2	2.4	1	3	0.3	6	6		82.35	38.99	62.76	6.4	
	3								82.35	62.71	62.71		5.98
	4								82.35	69.10	69.10		6.13
	5								82.35	72.90	72.90		6.21
	6								82.35	73.32	73.32		6.22
10	2	2.8	1	4	0.4	6	6		201.06	69.31	144.14	8	
	3								201.06	140.95	140.95		7.32
	4								201.06	158.01	158.01		7.53
	5								201.06	166.98	166.98		7.64
	6								201.06	167.99	167.99		7.65
12	2	3.5	1.5	5	0.4	6	6		416.92	157.70	297.92	9.6	
	3								416.92	294.51	294.51		8.80
	4								416.92	330.11	330.11		9.06
	5								416.92	348.00	348.00		9.18
	6								416.92	346.66	346.66		9.17
14	2	4.5	1.5	6	0.6	6	6		772.40	384.89	638.76	11.2	
	3								772.40	629.50	629.50		10.64
	4								772.40	706.52	706.52		10.95
	5								772.40	757.71	757.71		11.15
	6								772.40	785.39	785.39		11.25

From Figs. 5.1 and 5.2, apparently, the number of flutes affects the area moment of inertia of the cutting tool. Obviously, for a cutting tool, the area moment of inertia changes with the cutting flutes, the area moment of inertia increases with the number of flutes. For example, the area moment of inertia of a 3-flute cutting tool is smaller than

that of a 4-flute one. For a 3-flutes cutting tool, the area moment of inertia of the cutting tool can be very different from the approximate cutting tool because of the different design parameters of the cutting flutes.

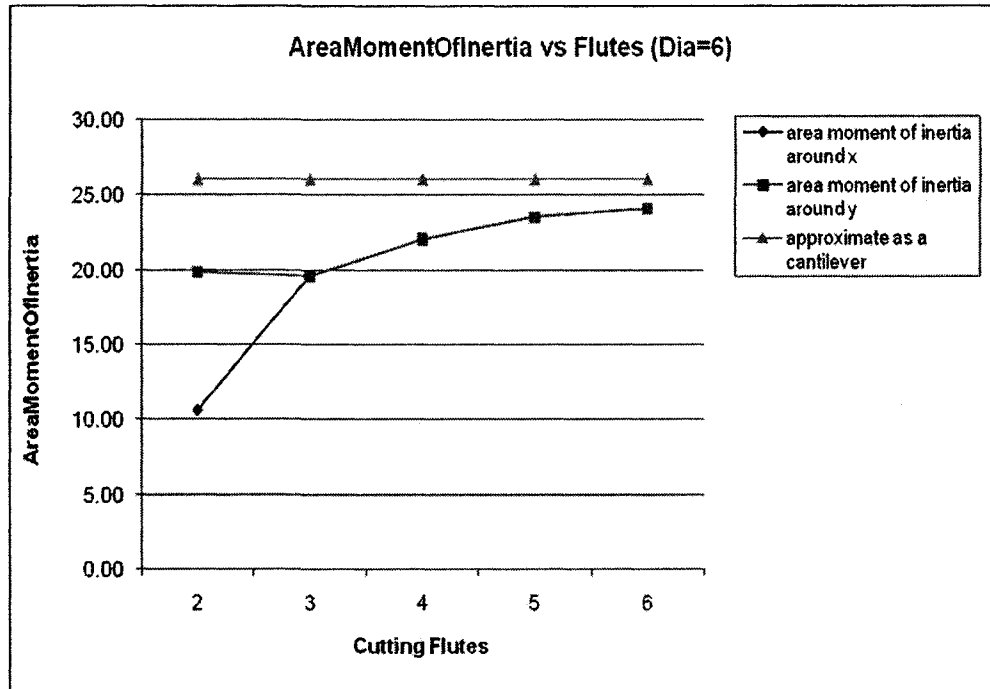


Figure 5-1 Area Moment of Inertia vs. Flutes.

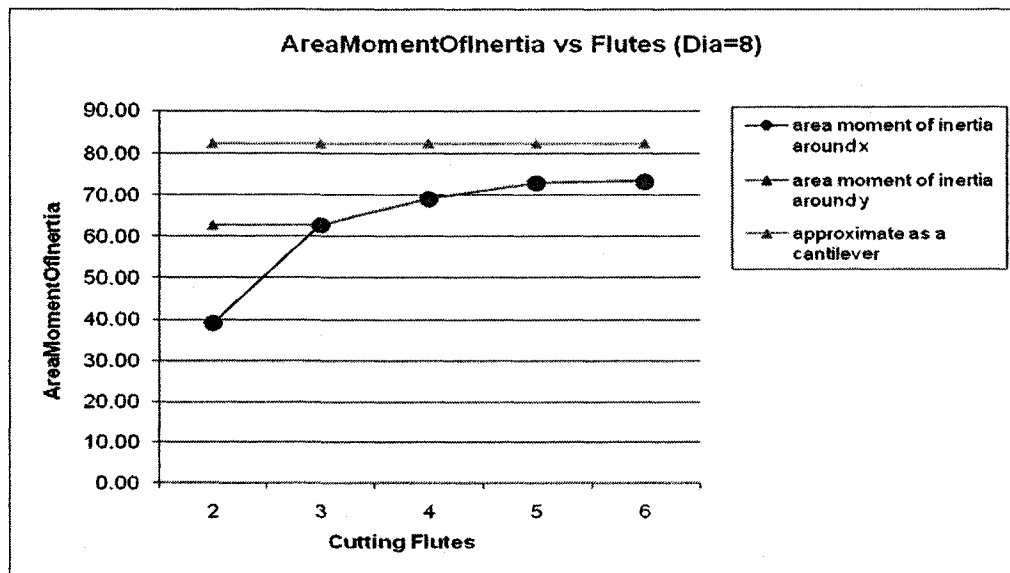


Figure 5-2 Area Moment of Inertia vs. Flutes.

5.3 Influence of the Other Parameters

In Section 5.2, a conclusion is made that the number of cutting flutes affects the area moment of inertia significantly. In this section, some other parameters will be considered as to how they affect the area moment of inertia. For example, the radius r_0 of the annular land on the end cutting surface is taken into consideration. Table 5.2 shows the comparison. Two 2-flutes cutting tool with different radius r_0 of the annular land on the end cutting surface are compared. With the change of the radius of the annular land, the area moment of inertia of the cutting tool changes too. The data for 3, 4, 5 and 6-flute cutting tools also shows the same result. To be clearer, the Fig. 5.3 illustrates the values in Table 5.2. The curves in blue and purple are the representations of area moment of inertia around the x axis and y axis, respectively, when r_0 is 3.5, while the green and yellow curves are the representations of inertia around the x axis and y axis when r_0 is 4.0. Table 3 shows that the influences of the radius of arc BC r_1 , the radius of arc CD r_2 , length_EF, rake angle γ_1 and relief angle γ_2 are minor, and not significant.

Table 5-2 Comparison of the Effect of the Radius of Annular Land r_0 on the Inertia

Parameters of Cutting Flute									Moment of Inertia			Effect Radius	Equivalent Radius
Dia. (mm)	Flute no.	r_0	r_1	r_2	l_{EF}	γ_1	γ_2	γ_3	Traditional	New Method			
										I_x	I_y		
12	2	3.5	1.5	5	0.4	6	6	45	416.92	157.69	297.92	9.6	
	2	4								233.65	350.83		
	3	3.5	1.5	5	0.4	6	6			294.51	294.51		8.80
	3	4								345.43	345.43		9.16
	4	3.5	1.5	5	0.4	6	6			330.11	330.11		9.06
	4	4								384.29	384.29		9.41
	5	3.5	1.5	5	0.4	6	6			348.00	348.00		9.18
	5	4								412.75	412.75		9.58
	6	3.5	1.5	5	0.4	6	6			346.66	346.66		9.17
	6	4								430.53	430.53		9.68

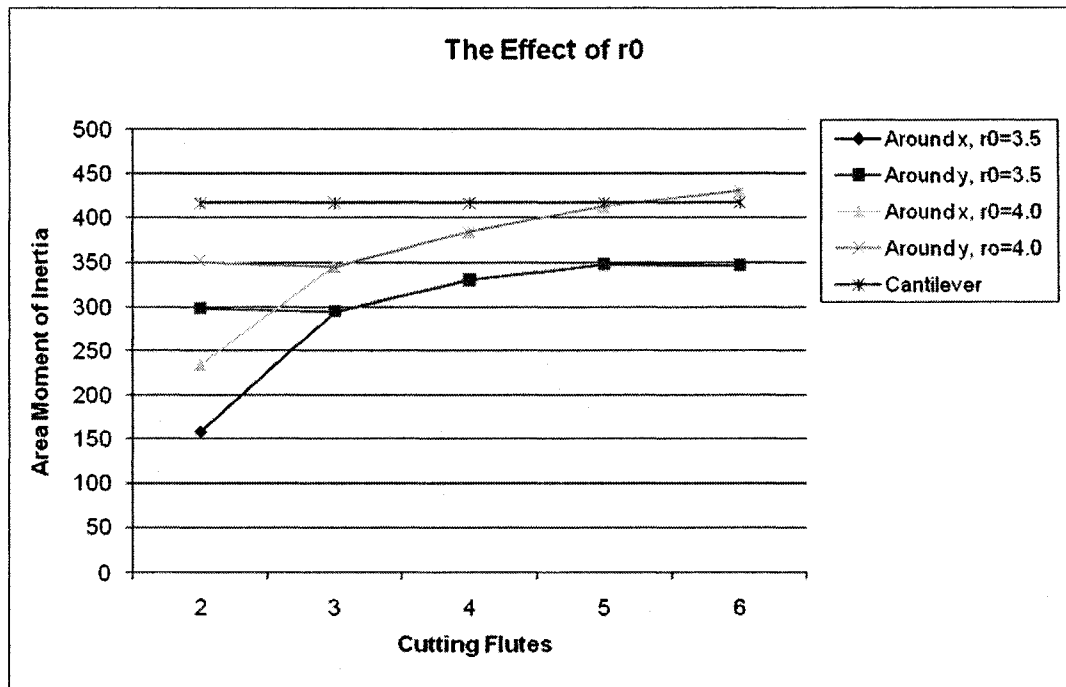
Figure 5-3 The Effect of r_0

Table 5-3 The Effect of r_1 , r_2 and Rake Angle, γ , and Relief Angle

Parameters of Cutting Flute									Moment of Inertia			Effect Radius	Equivalent Radius
Dia. (mm)	Flute no.	r_0	r_1	r_2	l_{EF}	γ_1	γ_2	γ_3	Traditional	New Method			
										I _x	I _y		
12	4	3.5	1.5	5	0.4	6	6	45	416.92	330.11	330.11	9.6	9.06
	4				0.45					336.15	336.15		9.10
	4	3.5	1.5	5	0.4	6	6			330.11	330.11		9.06
	4					5	5			332.38	332.38		9.07
	4	3.5	1.5	5	0.4	6	6			330.11	330.11		9.06
	4		1.8							330.59	330.59		9.06
	4		2.0							331.16	331.16		9.06
	4	3.5	1.5	6	0.4	6	6			324.44	324.44		9.02
	4			5						330.11	330.11		9.06
	4			4.5						333.04	333.04		9.08
4													

5.4 Along the Tool Axis, Different Position, Different Area

Moment of Inertia

For a symmetric section of a flat end-mill, at any position of the cutting edges along the tool axis, the area moments of inertia around the x and y axes are the same at the same layer. For example, for a 24 mm diameter cutting tool, $r_0 = 6$, $r_1 = 4$, $r_2 = 10$, $l_{EF} = 1$, $\gamma_1 = \gamma_2 = 6^\circ$, and $\gamma_3 = 45^\circ$, the area moments of inertia for at different positions are shown in Table 5-4. But for an asymmetric flat-end mill, not only is the area moment of inertia around the x axis different from around the y axis, but in the same direction, they are different at different position along the cutting tool axis. The curve shown in Figs. 5.4 and 5.5 are better demonstration of the data in Table 5-4

If consideration of the rotation of the spindle, for an asymmetric cutting tool, $n=2$, the area moment of inertia around x and y are repeated. In a cycle time, the area moment of inertia around x was covered by that around y , which are shown in Fig. 5.6. As shown in Table 5-5, for a symmetric section of an APT cutting tool, the area moments of inertia around the x axis equates to the area moments of inertia around the y axis, but obviously, for an asymmetric section of an APT cutting tool, the area moment of inertia around the x axis and y axis are not equal to each other. The curves in Fig. 5.7 and Fig. 5.9 are better demonstration of data in Table 5.5. Figs. 5.8 and 5.10 show the result of the area moment of inertia of an APT cutting tool when rotating the spindle.

Table 5-4 Data for Symmetric and Asymmetric Section Flat-End Mills

z	Symmetric Section (n=4)		Asymmetric Section (n=2)		
	Helix Lag Angle	Area Moment of Inertia Around $I_x=I_y$	Helix Lag Angle	Area Moment of Inertia Around I_x	Area Moment of Inertia Around I_y
0.1	0.0048	4525.8109	0.0048	1828.6242	4346.7011
0.2	0.0096	4525.8109	0.0096	1837.8823	4337.4431
0.3	0.0144	4525.8109	0.0144	1847.2560	4328.0694
0.4	0.0192	4525.8109	0.0192	1856.7446	4318.5808
0.5	0.0241	4525.8109	0.0241	1866.3471	4308.9782
0.6	0.0289	4525.8109	0.0289	1876.0628	4299.2626
0.7	0.0337	4525.8109	0.0337	1885.8906	4289.4348
0.8	0.0385	4525.8109	0.0385	1895.8297	4279.4957
0.9	0.0433	4525.8109	0.0433	1905.8792	4269.4462
1.0	0.0481	4525.8109	0.0481	1916.0380	4259.2873
1.1	0.0529	4525.8109	0.0529	1926.3054	4249.0200
1.2	0.0577	4525.8109	0.0577	1936.6803	4238.6451
1.3	0.0625	4525.8109	0.0625	1947.1618	4228.1636
1.4	0.0674	4525.8109	0.0674	1957.7488	4217.5766
1.5	0.0722	4525.8109	0.0722	1968.4405	4206.8849
1.6	0.0770	4525.8109	0.0770	1979.2358	4196.0896
1.7	0.0818	4525.8109	0.0818	1990.1338	4185.1916
1.8	0.0866	4525.8109	0.0866	2001.1333	4174.1920
1.9	0.0914	4525.8109	0.0914	2012.2335	4163.0919
2.0	0.0962	4525.8109	0.0962	2023.4333	4151.8921
2.1	0.1010	4525.8109	0.1010	2034.7316	4140.5938
2.2	0.1058	4525.8109	0.1058	2046.1273	4129.1980
2.3	0.1107	4525.8109	0.1107	2057.6196	4117.7058
2.4	0.1155	4525.8109	0.1155	2069.2072	4106.1182
2.5	0.1203	4525.8109	0.1203	2080.8891	4094.4363
2.6	0.1251	4525.8109	0.1251	2092.6642	4082.6612
2.7	0.1299	4525.8109	0.1299	2104.5314	4070.7940
2.8	0.1347	4525.8109	0.1347	2116.4897	4058.8357
2.9	0.1395	4525.8109	0.1395	2128.5379	4046.7875
3.0	0.1443	4525.8109	0.1443	2140.6749	4034.6505
3.1	0.1491	4525.8109	0.1491	2152.8996	4022.4258
3.2	0.1540	4525.8109	0.1540	2165.2108	4010.1146
3.3	0.1588	4525.8109	0.1588	2177.6075	3997.7179
3.4	0.1636	4525.8109	0.1636	2190.0884	3985.2370
3.5	0.1684	4525.8109	0.1684	2202.6524	3972.6730
3.6	0.1732	4525.8109	0.1732	2215.2984	3960.0270
3.7	0.1780	4525.8109	0.1780	2228.0251	3947.3003
3.8	0.1828	4525.8109	0.1828	2240.8314	3934.4939
3.9	0.1876	4525.8109	0.1876	2253.7162	3921.6092
4.0	0.1925	4525.8109	0.1925	2266.6781	3908.6472
4.1	0.1973	4525.8109	0.1973	2279.7161	3895.6093
...

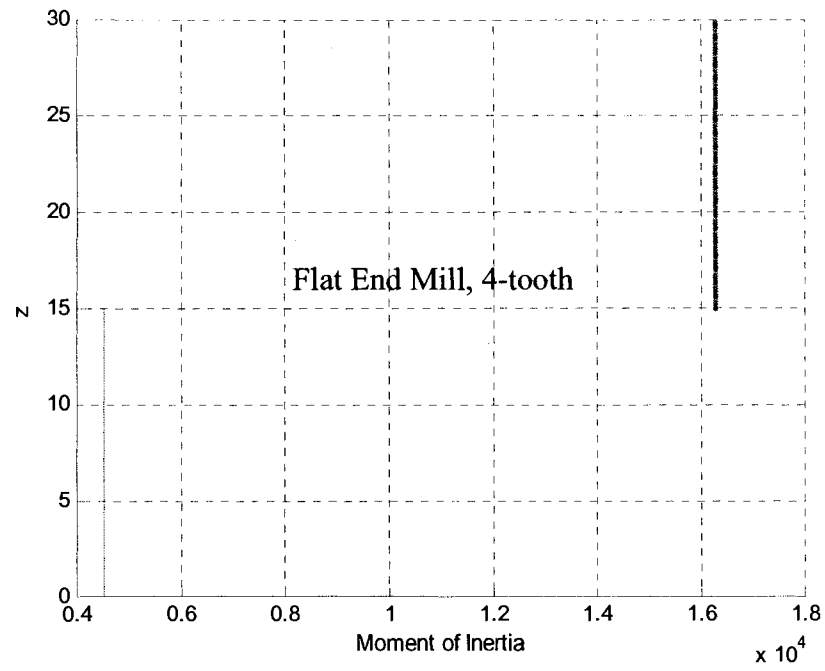


Figure 5-4 Area Moment of Inertia ~ z

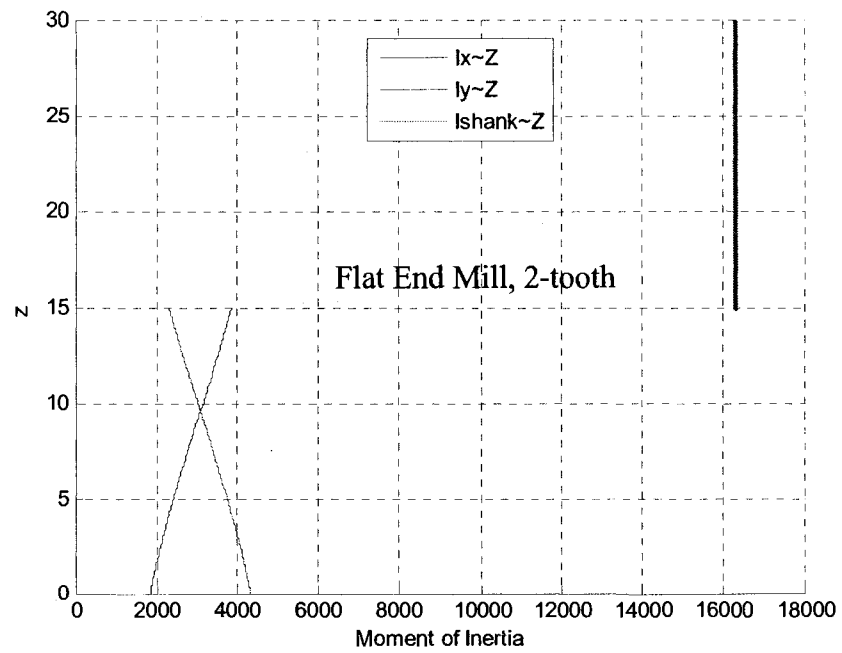


Figure 5-5 Area Moment of Inertia ~ z

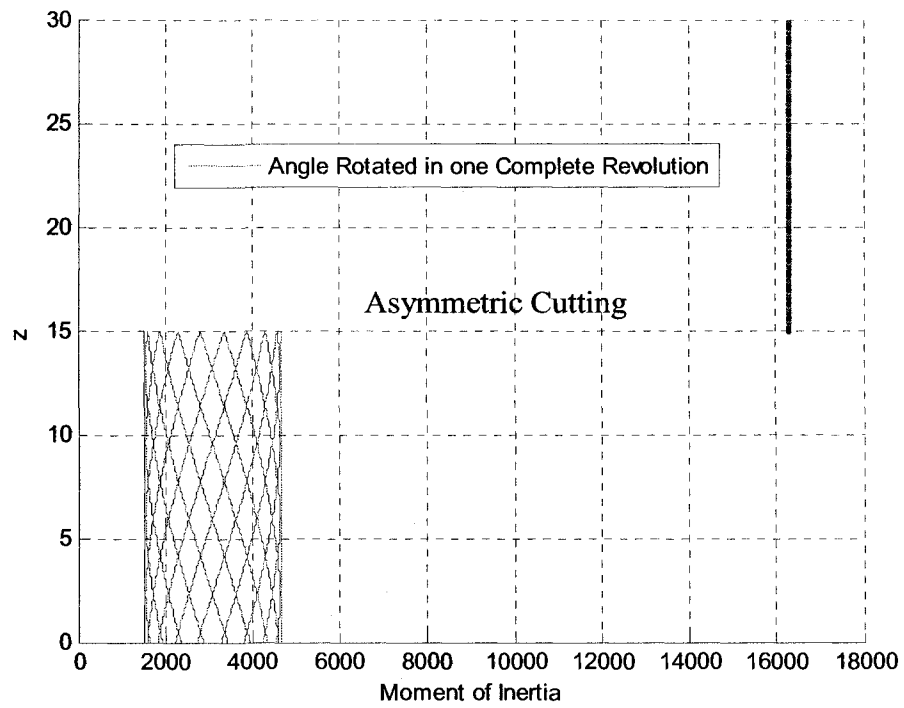
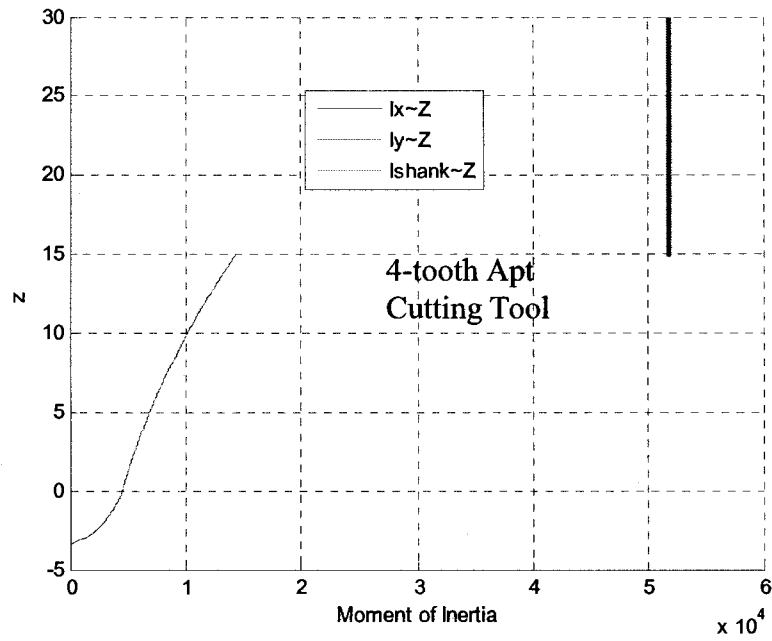
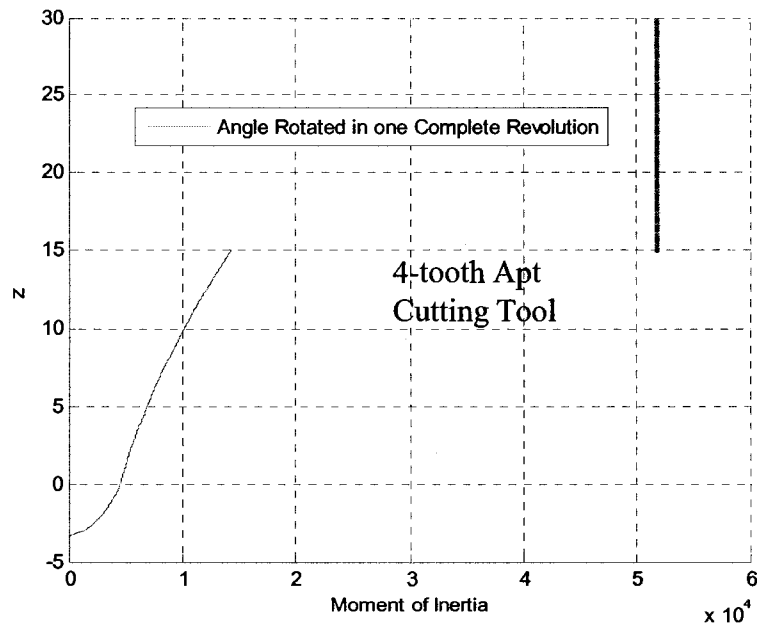


Figure 5-6 Area Moment of Inertia ~ z

Table 5-5 Data for Symmetric and Asymmetric Section APT Cutting Tool

z	APT, Symmetric Section (n=4)		APT, Asymmetric Section (n=2)		
	Helix Lag Angle	Area Moment of Inertia Around $I_x=I_y$	Helix Lag Angle	Area Moment of Inertia Around I_x	Area Moment of Inertia Around I_y
-3.7000	-1.8763	0.1948	-1.8763	0.2009	0.0649
-3.6000	-1.1947	4.3670	-1.1947	3.2362	2.7225
-3.5000	-0.8815	24.5901	-0.8815	12.9842	20.5683
-3.4000	-0.6782	81.8781	-0.6782	34.1126	77.6075
-3.3000	-0.5277	206.1858	-0.5277	74.4953	206.8387
-3.2000	-0.4082	436.4088	-0.4082	147.4094	448.0566
-3.1000	-0.3091	820.3834	-0.3091	273.2662	846.1209
-3.0000	-0.2245	1282.0062	-0.2245	435.7785	1313.4783
-2.9000	-0.1975	1544.6397	-0.1975	531.6326	1575.9792
-2.8000	-0.1807	1754.6337	-0.1807	609.4271	1784.7149
-2.7000	-0.1675	1939.7869	-0.1675	679.0123	1967.7654
-2.6000	-0.1564	2109.1929	-0.1564	743.5496	2134.3772
-2.5000	-0.1466	2267.1407	-0.1466	804.5113	2288.9303
-2.4000	-0.1377	2416.0316	-0.1377	862.7121	2433.8864
-2.3000	-0.1295	2557.3538	-0.1295	918.6504	2570.7777
-2.2000	-0.1218	2692.0942	-0.1218	972.6518	2700.6253
-2.1000	-0.1146	2820.9393	-0.1146	1024.9389	2824.1433
-2.0000	-0.1077	2944.3837	-0.1077	1075.6683	2941.8499
-1.9000	-0.1011	3062.7934	-0.1011	1124.9529	3054.1315
-1.8000	-0.0947	3176.4448	-0.0947	1172.8749	3161.2832
-1.7000	-0.0886	3285.5502	-0.0886	1219.4948	3263.5342
-1.6000	-0.0826	3390.2744	-0.0826	1264.8568	3361.0651
-1.5000	-0.0768	3490.7470	-0.0768	1308.9930	3454.0205
-1.4000	-0.0712	3587.0702	-0.0712	1351.9265	3542.5170
-1.3000	-0.0656	3679.3253	-0.0656	1393.6728	3626.6498
-1.2000	-0.0602	3767.5771	-0.0602	1434.2420	3706.4974
-1.1000	-0.0549	3851.8773	-0.0549	1473.6396	3782.1247
-1.0000	-0.0496	3932.2671	-0.0496	1511.8674	3853.5863
-0.9000	-0.0445	4008.7796	-0.0445	1548.9242	3920.9284
-0.8000	-0.0394	4081.4408	-0.0394	1584.8066	3984.1900
-0.7000	-0.0343	4150.2715	-0.0343	1619.5088	4043.4050
-0.6000	-0.0293	4215.2878	-0.0293	1653.0238	4098.6027
-0.5000	-0.0243	4276.5023	-0.0243	1685.3428	4149.8089
-0.4000	-0.0194	4333.9246	-0.0194	1716.4561	4197.0465
-0.3000	-0.0145	4387.5620	-0.0145	1746.3529	4240.3363
-0.2000	-0.0097	4437.4199	-0.0097	1775.0215	4279.6972
-0.1000	-0.0048	4483.5020	-0.0048	1802.4496	4315.1466
0.0000	0.0000	4525.8109	0.0000	1828.6242	4346.7011
0.1000	0.0050	4566.3694	0.0050	1854.6626	4376.0036
0.2000	0.0099	4607.1999	0.0099	1881.0870	4405.2911
0.3000	0.0149	4648.3036	0.0149	1907.9008	4434.5620
0.4000	0.0198	4689.6817	0.0198	1935.1072	4463.8147
...

Figure 5-7 Area Moment of Inertia $\sim z$ Figure 5-8 Area Moment of Inertia $\sim z$

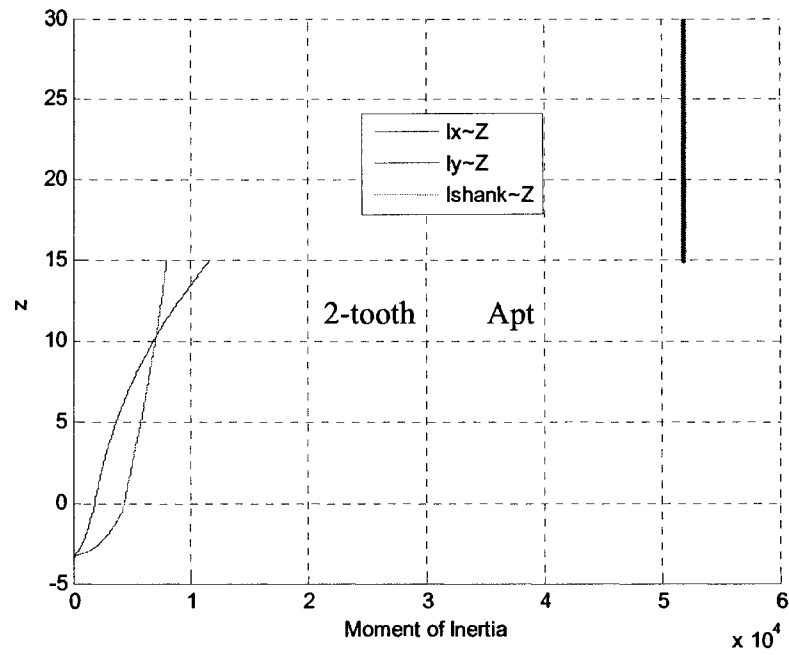


Figure 5-9 Area Moment of Inertia of a 2-tooth Apt Cutting Tool $\sim z$

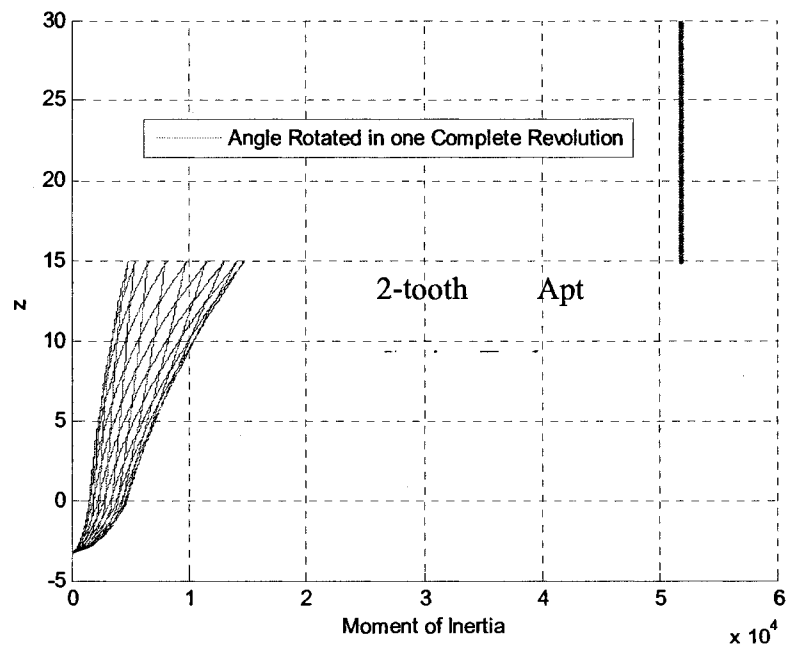


Figure 5-10 Area Moment of Inertia $\sim z$

Chapter 6 Results and Application

6.1 Introduction

In Chapter 5, we have concluded that the traditional way of considering the cutting tool as an approximate cantilever with an effective radius as 80% of the radius of the cutting tool is not accurate enough and showed some calculated area moments of inertia in the tables. To make these more convenience, in this chapter, an equivalent radius will be introduced. Equivalent radius means a virtual radius whose area moment of inertia equates to a certain cutting tool.

6.2 Applications

In this chapter, some of the equivalent radii and the area moments of inertia of cutting tools will be listed. All these data are based on the following assumptions.

1. Neglect the effect of the rake angle and relief angle and suppose these two angles are equal and both of them are six degrees. We have already shown that, in chapter 4, the influence of the rake angle and relief angle is not significant.

2. The declined angle of straight line DE (clearance angle) to the x axis γ_3 is 45 degrees.

In the real design of cutting tool, the value of r_0 , r_1 , r_2 and γ_3 should be defined by an optimal method according to the usage of the cutter.

Table 6.1, 6.2, and 6.3 are the area moments of inertia and their equivalent radii of some cutting tools which are frequently applied by the manufacturing industrial frequently. Also, the parameters of the sectional cutting flutes of the cutting tools are also listed for reference.

Table 6-1 Equivalent Radius for 2-Flute Cutters

Parameters of Flute									Moment of Inertia			Effect Radius	Equivalent Radius
Dia. (mm)	Flute no.	r0	r1	r2	l _{EF}	γ ₁	γ ₂	γ ₃	Traditional	New Method			
										I _x	I _y		
2	2	0.60	0.25	0.70	0.10	6	6	45	0.32	0.19	0.27	1.60	1.41
3		0.70	0.40	1.00	0.15				1.63	0.56	1.18	2.40	1.84
4		1.00	0.55	1.30	0.20				5.15	2.35	3.90	3.20	2.63
5		1.50	0.80	1.70	0.25				12.57	8.15	10.66	4.00	3.59
6		1.75	1.00	2.00	0.40				26.06	18.29	23.41	4.80	4.39
7		2.00	1.20	2.50	0.40				48.27	26.47	39.40	5.60	4.82
8		2.20	1.40	2.80	0.45				82.35	42.84	65.60	6.40	5.44
9		2.50	1.50	3.20	0.50				131.92	67.25	104.80	7.20	6.08
10		3.00	1.60	3.40	0.55				201.06	134.50	174.51	8.00	7.24
11		3.20	1.80	3.80	0.60				294.37	176.58	245.48	8.80	7.74
12		3.60	2.00	4.00	0.65				416.92	290.04	363.66	9.60	8.77
14		3.80	2.20	4.50	0.70				772.40	444.78	616.85	11.20	9.76
16		4.90	2.80	5.50	0.80				1317.68	841.83	1108.96	12.80	11.44
18		5.00	2.80	6.00	0.90				2110.67	1183.91	1688.22	14.40	12.46
20		6.00	3.50	7.00	1.00				3216.99	1983.55	2682.01	16.00	14.18
25		7.00	3.50	8.50	1.00				7853.98	3991.23	5964.54	20.00	16.89

Table 6-2 Equivalent Radius for 3-Flute Cutters

Parameters of Flute									Moment of Inertia			Effect Radius	Equivalent Radius
Dia. (mm)	Flute no.	r_0	r_1	r_2	l_{EF}	γ_1	γ_2	γ_3	Traditional	New Method			
										I_x	I_y		
2	3	0.65	0.25	0.80	0.10	6	6	45	0.32	0.28	0.28	1.60	1.55
3		0.70	0.40	1.20	0.15				1.63	1.01	1.01	2.40	2.13
4		1.00	0.60	1.60	0.20				5.15	3.40	3.40	3.20	2.89
5		1.50	0.80	2.00	0.25				12.57	10.10	10.10	4.00	3.79
6		1.75	1.00	2.50	0.40				26.06	21.55	21.55	4.80	4.58
7		2.25	1.20	2.80	0.40				48.27	43.51	43.51	5.60	5.46
8		2.50	1.50	3.25	0.45				82.35	71.69	71.69	6.40	6.18
9		2.70	1.70	3.60	0.50				131.92	109.38	109.38	7.20	6.87
10		2.80	1.80	4.00	0.55				201.06	153.36	153.36	8.00	7.48
11		3.20	2.00	4.50	0.60				294.37	233.10	233.10	8.80	8.30
12		3.50	2.25	5.00	0.65				416.92	330.01	330.01	9.60	9.06
14		4.00	2.50	5.00	0.70				772.40	602.61	602.61	11.20	10.53
16		5.00	2.75	6.00	0.80				1317.68	1128.35	1128.35	12.80	12.31
18		5.50	3.00	7.00	0.90				2110.67	1941.11	1941.11	14.40	14.10
20		6.50	3.50	8.00	1.00				3216.99	2862.38	2862.38	16.00	15.54
25		9.00	4.00	11.00	1.00				7853.98	9641.05	9641.05	20.00	21.05

Table 6-3 Equivalent Radius for 4-Flute Cutters

Parameters of Flute									Moment of Inertia			Effect Radius	Equivalent Radius
Dia. (mm)	Flute no.	r0	r1	r2	l _{EF}	γ ₁	γ ₂	γ ₃	Traditional	New Method			
										I _x	I _y		
2	4	0.60	0.25	0.80	0.10	6	6	45	0.32	0.28	0.28	1.60	1.55
3		0.80	0.40	1.20	0.15				1.63	1.26	1.26	2.40	2.25
4		1.00	0.60	1.60	0.20				5.15	3.66	3.66	3.20	2.94
5		1.50	0.80	2.50	0.25				12.57	10.87	10.87	4.00	3.86
6		1.75	1.00	3.00	0.40				26.06	23.02	23.02	4.80	4.65
7		2.25	1.25	3.50	0.40				48.27	47.05	47.05	5.60	5.56
8		2.50	1.50	4.00	0.45				82.35	77.27	77.27	6.40	6.30
9		2.75	1.75	4.25	0.50				131.92	120.42	120.42	7.20	7.04
10		3.00	1.80	4.50	0.55				201.06	178.96	178.96	8.00	7.77
11		3.25	2.00	4.75	0.60				294.37	257.28	257.28	8.80	8.51
12		3.50	2.25	5.25	0.65				416.92	357.52	357.52	9.60	9.24
14		4.00	2.50	6.00	0.70				772.40	636.42	636.42	11.20	10.67
16		5.00	2.75	7.00	0.80				1317.68	1215.02	1215.02	12.80	12.54
18		5.50	3.00	8.00	0.90				2110.67	1887.62	1887.62	14.40	14.00
20		6.00	3.75	9.00	1.00				3216.99	2816.69	2816.69	16.00	15.48
25		7.00	4.00	11.00	1.00				7853.98	7158.35	7158.35	20.00	19.54

Chapter 7 Conclusions and Future Research

7.1 Conclusions

In this work, a parametric modeling of APT cutters has been constructed in order to automatically and efficiently build 3-D solid model for end-mills, and a accurate approach to compute the area moments of inertia of the end-mills. More specifically, the research work includes: (1) establishment of a mathematical model of a helix curve cutting edge, (2) establishment of a standard mathematical model of a cutting flute, and (3) calculation of the area moment of inertia of the cutting tool. The purpose of building the mathematical model of the cutting tool is that, in all the current CAD/CAM software, the cutting tool is always represented by a solid model without flutes. This makes: (1) the prediction of machined error and deflection inaccurate, and (2) when simulating the machined surface in CAM software, the displayed machined surface is not accurate enough.

The data tables and figures are shown to clarify the difference of the area moment of inertia of the real design model of the cutting tool from the solid model without cutting flutes. The data tables and figures are clearly shown that the difference between the real

and the approximate models. Moreover, for more convenience, an equivalent radius conception is introduced and some of the equivalent radii of frequently used cutting tools in the manufacturing industrial with 2, 3, 4 flutes are listed. And, some other parameters of the cutting flutes are also listed. This work can be used, together with an existing cutting force calculation method, to accurately predict cutter deflections during milling in order to compensate them in CNC tool paths. It can also provide more precise 3-D solid models of end-mills for machining simulation by using finite element analysis.

7.2 Future Research

The following topics are suggested for a future work to expand the present research work:

- Using the built mathematic model to predict cutting force

In my current thesis, the mathematical model of cutting tool is built, which can be used in the visual machining and cutting force prediction.

- Using the built mathematic model to predict analyze of the stress of cutting tool
- The area moment of inertia can be applied into CAE software

In current trend software, the area moment of inertia is calculated by approximating the cutting tool as a cantilever. It is hoped this numerical method can be applied in the commercial software to predict the machined error and deflection.

Chapter 8 Appendix

Appendix I

This appendix is used to calculate the area moments of inertia around axes in a new coordinate system rotated relative to the original one. To calculate this, the product moment of area is required.

The area moments of inertia in any coordinate system can be calculated as

$$I_x = \int y^2 \cdot dA, \quad (8.1)$$

$$I_y = \int x^2 \cdot dA, \quad (8.2)$$

and, the product moment of area in the same coordinate system also can be calculated as

$$I_{xy} = \int x \cdot y \cdot dA, \quad (8.3)$$

respectively.

Considering the new coordinate system that is rotated relative to the original one by an angle, ϑ , then, the coordinates (x', y') in the new system can be calculated in terms of the coordinates (x, y) in the original one.

$$x' = x \cdot \cos \vartheta - y \cdot \sin \vartheta, \quad (8.4)$$

$$y' = x \cdot \sin \vartheta + y \cdot \cos \vartheta. \quad (8.5)$$

Substituting Eq. (8.4) and Eq. (8.5) into Eq. (8.1) and Eq. (8.2), the area moments of inertia around x' axis and y' axis can be obtained.

$$\begin{aligned} I_{x'} &= \int y'^2 \cdot dA = \int (x \cdot \sin \vartheta + y \cdot \cos \vartheta)^2 \cdot dA \\ &= \int ((y \cdot \cos \vartheta)^2 + (x \cdot \sin \vartheta)^2 + 2 \cdot x \cdot y \cdot \cos \vartheta \cdot \sin \vartheta) \cdot dA \\ &= \cos^2 \vartheta \cdot I_x + \sin^2 \vartheta \cdot I_y + 2 \cdot I_{xy} \cdot \cos \vartheta \cdot \sin \vartheta, \quad (8.6) \\ &= \frac{I_x}{2} \cdot (1 + \cos(2 \cdot \vartheta)) + \frac{I_y}{2} \cdot (1 - \cos(2 \cdot \vartheta)) + I_{xy} \cdot \sin(2 \cdot \vartheta) \\ &= \frac{I_x + I_y}{2} + \frac{I_x - I_y}{2} \cos(2 \cdot \vartheta) + I_{xy} \cdot \sin(2 \cdot \vartheta) \end{aligned}$$

$$\begin{aligned} I_{y'} &= \int x'^2 \cdot dA = \int (x \cdot \cos(\vartheta) - y \cdot \sin(\vartheta))^2 \cdot dA \\ &= \int ((x \cdot \cos \vartheta)^2 + (y \cdot \sin \vartheta)^2 - 2 \cdot x \cdot y \cdot \cos \vartheta \cdot \sin \vartheta) \cdot dA \\ &= \cos^2 \vartheta \cdot I_y + \sin^2 \vartheta \cdot I_x - 2 \cdot I_{xy} \cdot \cos \vartheta \cdot \sin \vartheta, \quad (8.7) \\ &= \frac{I_y}{2} \cdot (1 + \cos(2 \cdot \vartheta)) + \frac{I_x}{2} \cdot (1 - \cos(2 \cdot \vartheta)) - I_{xy} \cdot \sin(2 \cdot \vartheta) \\ &= \frac{I_x + I_y}{2} - \frac{I_x - I_y}{2} \cdot \cos(2 \cdot \vartheta) - I_{xy} \cdot \sin(2 \cdot \vartheta) \end{aligned}$$

Substituting Eq. (8.4) and Eq. (8.5) into Eq. (8.3), the product moment of area can be obtained.

$$\begin{aligned}
I_{xy'} &= \int x' \cdot y' \cdot dA \\
&= \int (x \cdot \cos \vartheta - y \cdot \sin \vartheta)(x \cdot \sin \vartheta + y \cdot \cos \vartheta) \cdot dA \\
&= \int \left((x^2 - y^2) \cdot \sin \vartheta \cos \vartheta + x \cdot y \cdot (\cos^2 \vartheta - \sin^2 \vartheta) \right) \cdot dA. \quad (8.8) \\
&= \int \left(\frac{(x^2 - y^2)}{2} \cdot \sin(2 \cdot \vartheta) + x \cdot y \cdot \cos(2 \cdot \vartheta) \right) \cdot dA \\
&= -\frac{I_x - I_y}{2} \cdot \sin(2 \cdot \vartheta) + I_{xy} \cdot \cos(2 \cdot \vartheta)
\end{aligned}$$

ϑ is the angle of rotation.

I_x , I_y and I_{xy} are the area moments of inertia and the product moment of area in the original coordinate system.

$I_{x'}$, $I_{y'}$ and $I_{xy'}$ are the area moments of inertia and the product moment of area in the rotated coordinate system.

Eq (8.9), (8.10) and Eq (8.11). were proved by Benham [15]. Apparently, they are the same expressions as Eq. (8.6), (8.7) and Eq. (8.8), respectively.

$$I_x^* = \frac{I_x + I_y}{2} + \frac{I_x - I_y}{2} \cos(2 \cdot \vartheta) + I_{xy} \cdot \sin(2 \cdot \vartheta) \quad (8.9)$$

$$I_y^* = \frac{I_x + I_y}{2} - \frac{I_x - I_y}{2} \cdot \cos(2 \cdot \vartheta) - I_{xy} \cdot \sin(2 \cdot \vartheta) \quad (8.10)$$

$$I_{xy}^* = -\frac{I_x - I_y}{2} \cdot \sin(2 \cdot \vartheta) + I_{xy} \cdot \cos(2 \cdot \vartheta) \quad (8.11)$$

ϕ is the angle of rotation.

I_x , I_y and I_{xy} are the area moments of inertia and the product moment of area in the original coordinate system.

I_x^* , I_y^* and I_{xy}^* are the area moments of inertia and the product moment of area in the rotated coordinate system.

Appendix II

Appendix II is to prove that, when a tool size is scaled by S , the area moment of inertia and the product moment of area should be scaled by S^4 .

The original width of the band is ΔR .

$$\rho = \rho_0 + (l - 0.5) \cdot \Delta R, \quad (8.12)$$

$$dA = \rho \cdot d\eta(\rho) \cdot \Delta R. \quad (8.13)$$

Area moment of inertia of each element around the x axis is

$$\begin{aligned} dI_x^m &= y^2 \cdot dA = \left(\rho \cdot \sin(\eta(\rho)) \right)^2 \cdot dA \\ &= \rho^3 \cdot \sin^2(\eta(\rho)) \cdot d\eta(\rho) \cdot \Delta R \end{aligned} \quad (8.14)$$

$$I_x = \sum dI_x^m. \quad (8.15)$$

Area moment of inertia of each element around the y axis is

$$\begin{aligned}
 dI_y^m &= x^2 \cdot dA = (\rho \cdot \cos(\eta(\rho)))^2 \cdot dA \\
 &= \rho^3 \cdot \cos^2(\eta(\rho)) \cdot d\eta(\rho) \cdot \Delta R
 \end{aligned}
 \tag{8.16}$$

$$I_y = \sum dI_y^m. \tag{8.17}$$

The product moment of area can be calculated.

$$\begin{aligned}
 dI_{xy}^m &= x \cdot y \cdot dA = \rho \cdot \cos(\eta(\rho)) \cdot \rho \cdot \sin(\eta(\rho)) \cdot dA \\
 &= \rho^3 \cdot \cos(\eta(\rho)) \cdot \sin(\eta(\rho)) \cdot d\eta(\rho) \cdot \Delta R
 \end{aligned}
 \tag{8.18}$$

$$I_{xy} = \sum dI_{xy}^m. \tag{8.19}$$

Supposing the tool size enlarged by S ; after enlargement, the width of the band would be enlarged to $\Delta R'$, then

$$\Delta R' = S \cdot \Delta R, \tag{8.20}$$

$$\rho' = S \cdot \rho, \tag{8.21}$$

$$\Delta\eta(\rho') = \Delta\eta(\rho) \tag{8.22}$$

$$d\eta(\rho') = \frac{\Delta\xi(\rho')}{na} = \frac{\Delta\eta(\rho)}{na} = d\eta(\rho), \tag{8.23}$$

$$dA' = \rho' \cdot d\eta(\rho) \cdot \Delta R', \tag{8.24}$$

Area moment of inertia of each element around the x axis is

$$\begin{aligned}
dI'_x &= y'^2 \cdot dA' = (\rho' \cdot \sin(\eta(\rho')))^2 \cdot dA' \\
&= \rho'^3 \cdot \sin^2(\eta(\rho)) \cdot d\eta(\rho) \cdot \Delta R' \\
&= (S \cdot \rho)^3 \cdot \sin^2(\eta(\rho)) \cdot d\eta(\rho) \cdot (S \cdot \Delta R), \\
&= S^4 \cdot (\rho^3 \cdot \sin^2(\eta(\rho)) \cdot d\eta(\rho) \cdot \Delta R) \\
&= S^4 \cdot dI_x^m
\end{aligned} \tag{8.25}$$

$$I'_x = \sum dI'_x = \sum S^4 \cdot dI_x^m = S^4 \cdot \sum dI_x^m = S^4 \cdot I_x^m. \tag{8.26}$$

Area moment of inertia of each element around the y axis is

$$\begin{aligned}
dI'_y &= x'^2 \cdot dA' = (\rho' \cdot \cos(\eta(\rho')))^2 \cdot dA' \\
&= \rho'^3 \cdot \cos^2(\eta(\rho)) \cdot d\eta(\rho) \cdot \Delta R' \\
&= (S \cdot \rho)^3 \cdot \cos^2(\eta(\rho)) \cdot d\eta(\rho) \cdot (S \cdot \Delta R), \\
&= S^4 \cdot (\rho^3 \cdot \cos^2(\eta(\rho)) \cdot d\eta(\rho) \cdot \Delta R) \\
&= S^4 \cdot dI_y^m
\end{aligned} \tag{8.27}$$

$$I'_y = \sum dI'_y = \sum S^4 \cdot dI_y^m = S^4 \cdot \sum dI_y^m = S^4 \cdot I_y^m. \tag{8.28}$$

For product moment of area, we also can prove this relation.

$$\begin{aligned}
dI'_{xy} &= x' \cdot y' \cdot dA' = \rho' \cdot \cos(\eta(\rho')) \cdot \rho' \cdot \sin(\eta(\rho')) \cdot dA' \\
&= \rho'^3 \cdot \cos(\eta(\rho)) \cdot \sin(\eta(\rho)) \cdot d\eta(\rho) \cdot \Delta R' \\
&= (S \cdot \rho)^3 \cdot \cos(\eta(\rho)) \cdot \sin(\eta(\rho)) \cdot d\eta(\rho) \cdot (S \cdot \Delta R), \\
&= S^4 \cdot \rho^3 \cdot \cos(\eta(\rho)) \cdot \sin(\eta(\rho)) \cdot d\eta(\rho) \cdot \Delta R \\
&= S^4 \cdot dI_{xy}^m
\end{aligned} \tag{8.29}$$

$$I'_{xy} = \sum dI'_{xy} = \sum S^4 \cdot dI_{xy}^m = S^4 \cdot \sum dI_{xy}^m = S^4 \cdot I_{xy}^m. \tag{8.30}$$

Chapter 9 Bibliography

- [1] S. Engin, and Y. Altintas, "Mechanics and dynamics of general milling cutters. Part I: helical end mills", *International Journal of Machine Tool & manufacture* 41 (2001) 2195-2212
- [2] W.-F. Chen, H.-Y. Lai and C.-K. Chen, "A Precision Tool Model for Concave Cone-End Milling Cutters", *Int J Adv Manuf Technol* (2001) 18:567-578
- [3] Ching-Ben Chen, Fu-Shou Wang, Pai-Chi Chang, Jia-Huei Hwang and Wei-Fang Chen, "A precision design and NC manufacturing Model for Concave-arc Ball-end Cutters", *Int J Adv Manuf Technol* (2006) 31: 283-296
- [4] Y. T. Wang, Q. S. Bao and Y. Y. Tang, "A Manufacturing Model of S-Shaped Ball-Nosed Milling Cutter and Error Analysis in Realization in Industry", *Int J Adv Manuf Technol* (2002) 20:92-98
- [5] C.-K. Chen and R.-Y. Lin, "A Study of Manufacturing Models for Ball-End Type Rotating Cutters with Constant Pitch Helical Flutes", *Int J Adv Manuf Technol* (2001) 18:157-167
- [6] S.-W. Lin and H.-Y. Lai, "A Mathematical Model for Manufacturing Ball-End Cutters Using a Two-Axis NC Machine", *Int J Adv Manuf Technol* (2001) 17:881-888

- [7] Ying-Chien Tsai, Jone-Ming Hsieh, "A study of a design and NC manufacturing model of ball-end cutters", *Journal of Materials Processing Technology* 117 (2001) 183-192
- [8] Wei-Fang Chen and Wei-Ya Chen, "Design and NC machining of a toroid-shaped revolving cutter with a concave-arc generator", *Journal of Materials Processing Technology* 121 (2002) 217-225
- [9] W-F Chen, "A mathematical solution to the design and manufacturing problems of ball-end cutters having a cutting edge with constant angle to the axis", *Proc. Instn Mech. Engrs Vol.218 Part C: J. Mechanical Engineering Science*
- [10] Jen-Yu Liu and Shinn-Lian Chang, "Design of hob cutters for generating helical cutting tools with multi-cutting angles" *International Journal of Machine Tools & Manufacture* 43 (2003) 1185-1195
- [11] D. S. Sheth, Eaton Corporation and S. Malkin, University of Massachusetts, "CAD/CAM for Geometry and Process Analysis of Helical Flute Machining", *Ann. CIRP* 22 (1) (1973) 157-164
- [12] S. Kaldor, Ada Mod Rafael and D. Messinger; Technion IIT, Haifa, "On the CAD of Profiles for Cutters and helical Flutes –Geometrical Aspects", *Ann. CIRP* 39(1), 129-132, 1990
- [13] S. K. KANG, K. F. EHMANN and C. LIN, "A CAD APPROACH TO HELICAL FLUTE MACHINING-I. MATHEMATICAL MODEL AND MODEL SOLUTION", *Int. J. Mach. Tools Manufact.* Vol. 36, No. 1, pp. 141-153, 1996
- [14] D. M. Rincon and A. G. Ulsoy, "Complex Geometry, Rotary Inertia and Gyroscopic Moment Effects on Drill Vibrations", *Journal of Sound and Vibration* (1995) 188(5), 701-715

[15] Benham, "Mechanics of Solids and Structures", P.P. ISBN: 0273361910

[16] Yusuf Altintas "Manufacturing Automation", P.P. ISBN: 0521659736